Inorganic Chemistry Communications 150 (2023) 110465

Contents lists available at ScienceDirect

Inorganic Chemistry Communications

journal homepage: www.elsevier.com/locate/inoche

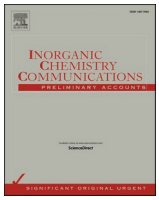

Short communication

Crystal structure, vibrational spectroscopy, ^{1}H NMR, and DFT analyses with antibacterial activity studies on silver nitrate complex of 5-iodoindole

Ceyhun Kucuk [a], Senay Yurdakul [a,*], Namık Özdemir [b], Belgin Erdem [c]

[a] Department of Physics, Gazi University, Ankara, Turkey
[b] Department of Mathematics and Science Education, Ondokuz Mayıs University, Samsun, Turkey
[c] Department of Health Care Services, Ahi Evran University, Kırşehir, Turkey

ARTICLE INFO

Keywords:
5-iodoindole silver nitrate complex
Vibrational spectra
DFT
Crystal structure
Antibacterial activity

ABSTRACT

A novel complex silver nitrate of 5-iodindole molecule has been synthesized and characterized by single-crystal X-ray diffraction, infrared and Raman spectroscopy, and ^{1}H NMR analysis. DFT calculations were performed using the B3LYP with 6–311++G(d,p) basis set for light atoms (C,H, N, and O) and the DGDZVP basis set for heavy atoms (Ag and I). Theoretical and experimental bond lengths and bond angles have been compared and determined to be in good agreement with each other. By using ^{1}H NMR analysis, the chemical shift values of H atoms in this new structure were determined and compared with the theoretically calculated values. Also, experimental FT-IR and FT-Raman modes of the complex structure assigned that depending on total energy distribution (TED) values have been compared with theoretical wavenumbers. The HOMO-LUMO energy gap, the frontier molecular orbital, the molecular electrostatic potential map, and atomic charge analysis have been carried out to reveal the electronic properties of the structure. The non-linear optical properties of the title molecule and its thermodynamic properties such as entropy, heat capacity, enthalpy change, and Gibbs free energy at different temperatures were investigated. Finally, the antibacterial activity of this new structure obtained from the synthesis of 5-iodoindole with silver nitrate has been evaluated.

1. Introduction

The indole core is the main component of many important compounds that are found in nature and have biological activity. Due to its various biological activities and pharmacological importance, it is widely used in the discovery of new drugs with different modes of action [1]. The indole alkaloids and their derivatives exhibit anticancer [2], antimicrobial [3], antiviral [4], antimalarial [5], anti-inflammatory [6], antihypertensive [7], antidiabethic [8], anti-Parkinson's [9], and antioxidant [10] activities. There are many indole-containing drugs available on the market. For example, indomethacin is a non-steroidal anti-inflammatory drug that is used to reduce fever, pain, and inflammation [11]. Reserpine is used for the treatment of high blood pressure [12]. Arbitol is used for the treatment of influenza A and B viruses, respiratory syncytial viruses, and SARS [13–15]. Vinblastine is a chemotherapy drug used in combination with other drugs to treat a number of cancer types [16]. Ergotamine which contains an indole scaffold in its structure is used in the treatment of migraine and mammary carcinoma treatment [17]. Tulongisin, which has antibacterial, anti-HIV, cytotoxic and antibiotic effects, contains indole alkaloid [18]. Also, indole and analogs are used as plant growth regulators and as fungicidal, insecticidal, and herbicidal agents in agriculture [16].

The use of transition metal complexes as reagents for the synthesis of complex organic compounds has increased considerably in recent years. Metal ions can be surrounded by free ligands, which determine the reactivity in the desired direction, and metal complexes are formed in ionic or neutral [19]. Transition metals play an important role in the development of metal-based drugs to treat various diseases such as carcinomas, lymphomas, diabetes, neurological disorders, and inflammation [20]. By providing reactivity with different ligands, the properties of metal ions can be materialized as desired, and new metal-based drugs can be designed [19]. Due to the high antimicrobial activity and non-toxic effect on humans of silver among transition metal ions, use as an antimicrobial has recently attracted attention again. Silver complexes are as effective against bacteria as broad-spectrum antibiotics, as antibiotics have recently failed against bacteria, bacteria have developed resistance to synthetic antibiotics, and synthetic antibiotics have more side effects [21]. In addition, silver complexes are used as antiseptic,

* Corresponding author.
E-mail address: senayy@gazi.edu.tr (S. Yurdakul).

https://doi.org/10.1016/j.inoche.2023.110465
Received 2 October 2022; Accepted 29 January 2023
Available online 2 February 2023

antitumor, and anticancer agents [22–24].

In the literature, there are experimental and theoretical studies of many metal complexes of indole ligand. Joseyphus and Nair synthesized the Co (II), Ni (II) and Cu (II) complexes of indole-3-carboxaldehyde and conducted characterization and biological activity studies in 2010 [25]. In another study, complexes of 2-methylindole and 2.5dimethylindole alkyldolyls coordinated through the nitrogen atom in the form of 3H-indole were isolated and characterized by X-ray crystal structure analysis and spectroscopic methods [26]. In this study, complex structures of 5-iodoindole ($Ag_2(NO_3)_2(C_8H_6IN)_2$), an indole derivative, were formed with silver nitrate and structural, spectroscopic, electrical, thermodynamic, and optical properties were investigated. In addition, the antibacterial activities of the synthesized complex were evaluated. A full structural analysis was performed by comparing the geometric optimized structure, vibration frequencies, ^{1}H NMR chemical shifts, and UV–Visible spectrum analyses obtained by the DFT method with experimental methods.

2. Material and methods

2.1. Computational methods

Computer-based calculations were made using the Gaussian 09 W and visualized using the Gauss View 5.0 package program [27,28]. The initial geometry of the synthesized complex structure obtained from the XRD data was used in the optimization analysis. The ground state geometry optimization calculations were performed in density functional theory with the Becke-3-Lee-Yang-Parr (B3LYP) by applying the 6–311++G(d,p) basis sets for carbon, nitrogen, oxygen, and hydrogen atoms and the DGDZVP for the silver and iodine atoms. The DGDZVP (Density Gauss Double-Zeta with Polarization functions), known as the full electron basis set, is a suitable choice for calculating X-I bond length, X-I IR vibration, and iodination reaction enthalpy values of organic compounds [29]. It is also used in the calculations of structures containing silver atoms [30,31]. Using the same basis sets, vibrational, frontier orbital, molecular electrostatic potential surface, charges, nonlinear optical property and thermodynamic properties at different temperatures were analyzed over the optimized structure. The ^{1}H NMR chemical shifts analyses of the title molecule were calculated and reported in ppm relative to TMS at the 6–311++(2d,p) for light atoms and the DGDZVP level for heavy atoms by using the Gauge Independent Atomic Orbital (GIAO) [32]. Using the Crystal Explorer 17 program, Hirshfeld surfaces were mapped and two-dimensional fingerprint drawings were created [33].

2.2. Experimental methods

2.2.1. Synthesis method

5-iodoindole and silver nitrate were supplied by Sigma Aldrich Chemical Company and were used without additional purification. The silver complex structure of 5-iodoindole was synthesized through a chemical process. The $AgNO_3$ (169 mg, 1 mmol) was liquefied in 10 ml of ethanol and was gradually added to a solution of 5-iodoindole in 10 ml of ethanol (486 mg, 2 mmol). After stirring for 2 h, the mixture was filtered and covered with aluminum foil to protect it from light. The mixture was kept at + 4 °C for 3 months, and the colorless and translucent $Ag_2(NO_3)_2(C_8H_6IN)_2$ crystals were obtained at the end of this period.

2.2.2. Spectroscopic and ^{1}H NMR measurement

The infrared spectrum was recorded in the range of 4000 cm^{-1} and 550 cm^{-1} by using a Bruker FT-IR spectrometer that has ATR equipment. Also, the Raman spectrum was recorded between 4000 cm^{-1} and 100 cm^{-1} by using a Jasco FT-Raman spectrometer with an NRS400 confocal microscope. The ^{1}H NMR spectrum of the title complex was recorded with chemical shifts in the range of 0–15 ppm (δ) in the chloroform solvent at room temperature using the Bruker Ultrashield 300 MHz spectrometer.

2.2.3. Determination of antimicrobial activity by agar well diffusion method

Escherichia coli ATCC 25922, *Klebsiella* pneumoniae ATCC 13883, *Shigella* dysenteriae ATCC 11835, *Pseudomonas* aeruginosa ATCC 27853, *Salmonella* typhimurium ATCC 14028, *Bacillus*. subtilis ATCC 6633, *Staphylococcus* aureus ATCC 25923, *Enterococcus* faecalis ATCC 29212, *Listeria* monocytogenes ATCC 764, and Candida albicans ATCC 10231, obtained from *Kırsehir* Ahi Evran University, Biology Department's Culture Collection Laboratory were used. Test bacteria were inoculated into Nutrient Broth (Difco) and incubated for 24–48 h. Mueller Hinton Agar (Oxoid) was used in the agar well diffusion method and to count bacteria and yeasts (10^6 per mL) for 24–48 h. The wells of the culture plates were drilled with a sterile cork borer (7 mm diameter). A stock solution of each of the synthesized compounds (1.0 mg/mL) in ethyl alcohol was prepared and graded dilutions of the tested compounds were placed in corporate in a cavity (depth 3 mm, diameter 4 mm) made in the center of the Petri dish (Mueller Hinton Agar for bacteria and Sabouraud dextrose agar medium for yeast). The plates were incubated in duplicates for 48 h at 37 °C (for bacteria) and at 30 °C (for yeasts). The diameter of the zone of inhibition generated by each of the test compounds against bacterial and yeast growth was measured using the antibiogram zone measuring scale. A positive control using inoculation and a negative control using ethyl alcohol were carried out. Ethyl alcohol (1 mg/mL) dissolved compounds (75 μL) were added to these wells. After 24–48 h, the inhibition zones formed on the agar plates were measured in millimeters (mm). Ampicillin and Cycloheximide were used as positive controls, and ethyl alcohol was used as a negative control. The NCCLS guideline was used for each step of the disk diffusion method [34]. Antimicrobial activity was evaluated according to the diameter of the clear inhibition zone around the well. The absence of an inhibition zone indicates no antimicrobial activity. Trials were repeated three times, and the results represent the average of three independent experiments.

2.2.4. Determination of antimicrobial activity by minimum inhibitory concentration

Minimum inhibitory concentrations (MIC) for compounds against test bacteria and yeast strains were examined in accordance with the NCCLS guideline [35]. Mueller-Hinton broth was used in suspension of bacteria (0.5 McFarland), in solutions of substances to be tested (1000 μg/ml in ethyl alcohol) and in MIC testing. Antimicrobial effects of synthesized compounds: minimum inhibitory concentration (MIC) values were found and tested. MIC values were determined spectrophotometrically in 96-well microtiter plates according to the microdilution broth method. MIC measurements for the antimicrobial effect test, 1 mg/mL stock solutions of the synthesized compounds in ethyl alcohol were prepared. Bacteria and yeast stock cultures were prepared according to the McFarland 05 turbidity standard, containing 106 cfu/ml of bacteria and yeast. Fresh bacterial growths (18 h) were standardized to the 0.5 Mac Farland standard in nutrient broth, which was then used as an inoculum. In 96-well plates containing 100 μL of 500, 250, 125, 62.5, 31.2, and 15.6 μg/mL of compounds, 100 μL of inoculum were seeded in duplicate and allowed to grow overnight with flow at 37 °C. For MIC determination by the Microdilution Broth method, a 96-well sterile 100 μL of NB medium was added to all wells of the microtiter plates with an automatic dispenser device (BioTek, Micro Fill). The absorbance at 590 nm wavelength was measured with a microplate reader (BioTek, μQuant) of plates incubated at 37 °C for 24 h. Ethyl alcohol was used as a negative control. The positive control contains the microorganisms.

2.2.5. X-ray crystallography

X-ray data of $Ag_2(NO_3)_2(C_8H_6IN)_2$ were collected with a STOE IPDS

II diffractometer at room temperature using graphite-monochromated Mo Kα radiation by applying the ω-scan method. Data collection and cell refinement were carried out using X-AREA [36] while data reduction was applied using X-RED32 [36]. The structure was solved using the charge-flipping algorithm by SUPERFLIP [37] and refined by means of the full-matrix least-squares calculations on F^2 using SHELXL-2018 [38]. All H atoms were placed geometrically and treated using a riding model, fixing the bond lengths at 0.86 and 0.93 Å for NH and CH atoms, respectively. The displacement parameters of the H atoms were fixed at $U_{iso}(H) = 1.2U_{eq}$ of their parent atoms. Crystal data, data collection and structure refinement details are given in Table 1. Molecular graphics were generated by using OLEX2 [39].

3. Results and discussion

3.1. Description of structure

The solid-state structure of $Ag_2(NO_3)_2(C_8H_6IN)_2$ has been unambiguously determined by single crystal X-ray analysis. Molecular structure of the complex is illustrated in Fig. 1, while geometric parameters are listed in Table 2. The structure contains two different Ag^+ ions. The first silver cation, Ag_1, is pentacoordinated in a propeller arrangement as it is bound to one iodine atom, two oxygen atoms from two different nitrate groups and two carbon atoms of a C=C bond of the 5-iodoindole. However, the second cation, Ag_2, is hexacoordinated and complexed by one iodine atom, three oxygen atoms from two different nitrate groups and two carbon atoms of a C=C bond of the 5-iodoindole. The formal coordination number of Ag_1 is four, while it is five for Ag_2. The Ag—O distances range from 2.389(5) to 2.669(4) Å, which are shorter than the sum of the van der Waals radii of silver and oxygen (3.24 Å). The 5-iodoindole ligand is coordinated to the silver atom in an asymmetric η^2 fashion. One of the Ag—C bonds is short [Ag_1—C_2 = 2.409(5) Å and Ag_2—C_{10} = 2.495(5) Å], while the other is relatively longer [Ag_1—C_1 = 2.591(5) Å and Ag2—C9 = 2.680(6) Å], however, all are shorter than the sum of the van der Waals radii of silver and carbon (3.42 Å). The Ag—I distances vary from 2.7489(6) to 2.8600(6) Å, which are shorter than the sum of the van der Waals radii of silver and iodine (3.70 Å).

If X_1 and X_2 are defined as the midpoint of the C_1=C_2 and C_9=C_{10} alkene bond of the 5-iodoindole ligands, the Ag_1—X_1 and Ag_2—X_2 distances are found to be 2.4063(5) and 2.4968(5) Å, respectively. In addition, the $I2^{ii}$—Ag_1—X_1, O_1—Ag_1—X_1 and O_4^{i}—Ag_1—X_1 angles are 149.75(2), 98.36(11) and 86.49(11)° while the I_1^{ii}—Ag_2—X_2, O_2—Ag_2—X_2, O_3—Ag_2—X_2 and O_4—Ag_2—X_2 angles are 122.47(2), 90.65 (12), 99.98(12) and 132.68(10)°, respectively. For quantitative evaluation of the extent of distortion around silver(I) centers, the structural indexes τ_4 [40] and τ_4' [41]were employed for atom Ag1, while the τ_5 [42] geometry index was used for atom Ag_2.

$$\tau_4 = \frac{360^o - (\alpha + \beta)}{360^o - 2\theta} \quad (1)$$

$$\tau'_4 = \frac{\beta - \alpha}{360^o - \theta} + \frac{180^o - \beta}{180^o - \theta} \quad (2)$$

$$\tau_5 = \frac{\beta - \alpha}{60^o} \quad (3)$$

where α and β (β > α) are the two greatest valence angles and θ is the ideal tetrahedral angle (109.5°). The τ_4 (and τ_4') value for ideal square-planar and tetrahedral coordination spheres is 0 and 1, respectively. For five-coordinate structures, same values correspond to the τ_5 values of square-pyramidal and trigonal bipyramidal geometries, respectively. The calculated geometry indices for the Ag_1 atom are $\tau_4 \approx 0.699$ and $\tau_4' \approx 0.581$, whilst the structural index parameter for the Ag_2 atom is $\tau_5 \approx 0.054$. It can be seen clearly that Ag1 is closer to a distorted tetrahedral arrangement, as the value of the structural index for Ag_2 points out a slightly distorted square-pyramidal geometry.

The $Ag_2(NO_3)_2(C_8H_6IN)_2$ unit forms linear 1D infinite coordination polymers along [0 1 0] (Fig. 2a). Within a polymer, only a C—H···O interaction exists in which atom *C*2 at (x, y, z) acts as a hydrogen-bond donor to atom O6 at (−x + 2, −y, −z + 1). Adjacent polymers are interconnected by one C—H···O and three N—H···O interactions (Fig. 2b). In this connection, atom N2 at (x, y, z) acts as hydrogen-bond donor to atoms O1 and O2 at (−x + 1, −y, −z + 1), so forming a centrosymmetric $R_1^2(4)$ ring motif [43]. Furthermore, atoms N1 and C7 at (x, y, z) act as hydrogen-bond donor to atoms O5 and O6 at (−x + 1, −y, −z + 1), respectively, together producing a second centrosymmetric $R_2^2(8)$ ring motif. Full details of the hydrogen-bonding geometry are given in Table 3.

3.2. Optimized molecular structure

The optimized molecular geometry of the title complex structure was calculated using B3LYP/6–311++G(d,p) with DGDZVP level of theory. These calculations were made in the gas phase and the initial geometries were taken from the X-ray data. The computed structural bond lengths and bond angles parameters are listed in Table 2 and compared with XRD data. Also, the optimized molecular structure are presented in Fig. 1. Most of the calculated bond lengths were found slightly longer than the X-ray values. In particular, a significant deviation was observed between the theoretical and experimental Ag_2—C_9 and Ag_2—C_{10} bond lengths. When the theoretical and experimental bond angle values are compared, the these values of the benzene and pyrrole rings of 5-iodoindole ligands in the complex structure are quite compatible with each other. There are observed more deviations between the theoretical and experimental values for the O_1—Ag_1—C_2, O_4—Ag_2—O_3, and O_2—Ag_2—C_{10} bond angles. We can say that the reason for these deviations is that the experimental results correspond to molecules interacting in the crystal lattice, while the calculation method deals with an isolated molecule in the gas phase. Correlation graphics for theoretical and experimental bond lengths and bond angles were given in supplementary Fig. S1.

Table 1
Crystal data and structure refinement parameters for $Ag_2(NO_3)_2(C_8H_6IN)_2$.

CCDC depository	2,043,732
Color/shape	Colorless/prism
Chemical formula	$[Ag_2(NO_3)_2(C_8H_6IN)_2]$
Formula weight	825.84
Temperature (K)	296(2)
Wavelength (Å)	0.71073 Mo Kα
Crystal system	Triclinic
Space group	$P\,\bar{1}$ (No. 2)
Unit cell parameters	
a, *b*, *c* (Å)	9.0698(4), 10.9367(4), 11.8151(5)
α, *β*, *γ* (°)	115.855(3), 91.526(3), 100.801(3)
Volume (Å^3)	1028.17(8)
Z	2
$D_{calc.}$ (g/cm^3)	2.668
μ (mm^{-1})	4.950
Absorption correction	Integration
$T_{min.}$, $T_{max.}$	0.1854, 0.5192
F_{000}	768
Crystal size (mm^3)	0.65 × 0.32 × 0.17
Diffractometer	STOE IPDS II
Measurement method	*ω* scan
Index ranges	$-11 \le h \le 11$, $-14 \le k \le 14$, $-15 \le l \le 15$
θ range for data collection (°)	$2.765 \le \theta \le 27.706$
Reflections collected	23,620
Independent/observed reflections	4808/4348
$R_{int.}$	0.0424
Refinement method	Full-matrix least-squares on F^2
Data/restraints/parameters	4808/0/271
Goodness-of-fit on F^2	1.147
Final *R* indices [$I > 2\sigma(I)$]	$R_1 = 0.0391$, $wR_2 = 0.0903$
R indices (all data)	$R_1 = 0.0448$, $wR_2 = 0.0932$
$\Delta\rho_{max.}$, $\Delta\rho_{min.}$ (e/Å^3)	1.43, −0.91

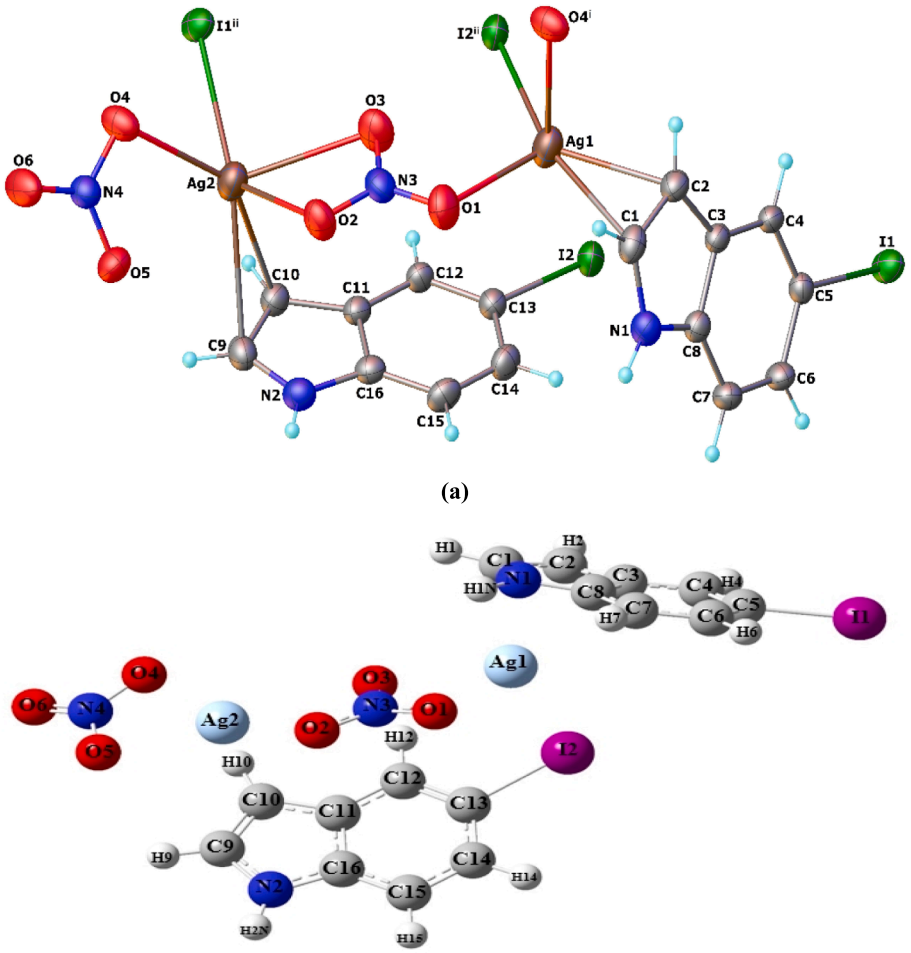

Fig. 1. **(a)** A view of the asymmetric unit of $Ag_2(NO_3)_2(C_8H_6IN)_2$, with atom labelling [symmetry codes: (i) $-x+2, -y, -z+1$; (ii) $-x+2, -y+1, -z+1$] and **(b)** optimized molecular structure. Displacement ellipsoids are drawn at the 30 % probability level.

According to these graphs, theoretical and experimental bond lengths and bond angles are in high agreement with each other.

3.3. Vibrational spectral analysis

The title complex structure $Ag_2(NO_3)_2(C_8H_6IN)_2$ has 42 atoms and 120 vibrational modes. Theoretical and experimental vibrational wavenumbers, IR, and Ra intensities with total energy distribution (TED) values are listed in Table 4. Also, experimental Far-IR spectra of 5-iodoindole and its silver nitrate complex and the recorded FT-IR and FT-Ra spectra of silver nitrate complex are given in supplementary Fig. S2. The correlation graphs are presented to determine the agreement between the theoretical and experimental wavenumbers in Fig. 3. Due to the fact that theoretical wavenumber values are higher than experimental, scale factors were used to harmonize the theoretical and experimental values. A scale factor of 0.997 was used for wave numbers below 1800 cm^{-1} [44], while a scale factor of 0.955 was used for wave numbers above 1800 cm^{-1} [45].

The characteristic N—H stretching modes are observed in the range of 3500–3000 cm^{-1} [46]. The N—H stretching vibration values of the title complex were calculated at 3499 and 3484 cm^{-1}. Experimental values were observed at 3412 cm^{-1} (w, IR)/3411 cm^{-1} (s,Ra) and 3280 cm^{-1} (w, IR)/3340 cm^{-1} (vw, Ra) in the FT-IRand FT-Ra spectra. In the literatüre, the N—H stretching vibration mode of indole and 5-iodoindole molecules were recorded at 3412 cm^{-1} in the FT-IR spectrum [47,48].

The C—H stretching vibration values of heteroaromatic compounds are found in the range of 3100 cm^{-1}-3000 cm^{-1} [49]. Calculated C—H stretching vibrations were found to be 3116 cm^{-1}, 3106 cm^{-1}, 3095 cm^{-1}, 3081 cm^{-1}, 3065 cm^{-1}, 3054 cm^{-1}, 3041 cm^{-1}, 3037 cm^{-1}. These modes were experimentally determined at 3102 cm^{-1} (w, IR)/ 3112 cm^{-1} (w, Ra), 3069 cm^{-1} (m, Ra), 2956 cm^{-1} (vw, IR). The C—H stretching vibrations for indole molecule were found to be 3099 cm^{-1} in the FT-IR spectrum [47]. In the frequency analysis that was previously performed for the free 5-iodoindole ligand, the C—H stretching vibrations were observed at 3100 cm^{-1}, 2988 cm^{-1}, and 2902 cm^{-1} in the FT-IR spectrum and at 3114 cm^{-1} and 3062 cm^{-1} in the FT-Ra spectrum. Also these vibrations were calculated at 3108 cm^{-1}, 3090 cm^{-1}, 3058 cm^{-1}, 3049 cm^{-1}, and 3026 cm^{-1} by using same basis set for 5-iodoindole [48].

The in-plane and out-plane C—H bending vibrations appear in the range of 1000 cm^{-1}-1300 cm^{-1} and 750 cm^{-1}-1000 cm^{-1}, respectively [50]. In plane C—H bending vibration of the title complex were observed at 1057 (m, IR), 1072 (w, Ra), 1091 (m, IR), 1135 (m, IR)/ 1131 (vw, Ra), 1191 (s, IR)/1191 (vw, Ra), 1236 (s, IR)/1250 (m, IR), 1287 (vs IR), 1330 (s, IR)/1332 (s, Ra) in the FT-IR and FT-Ra spectra. In addition, the theoretical values corresponding to observed vibration values are 1061 cm^{-1}, 1070 cm^{-1}, 1092 cm^{-1}, 1124 cm^{-1}, 1206 cm^{-1}, 1265 cm^{-1}, 1281 cm^{-1}, 1330 cm^{-1}. These vibration modes for 5-iodoindole ligands were calculated at 1282, 1268, 1209, 1161, 1108 cm^{-1}, and 1087 cm^{-1} and observed at 1261 cm^{-1},1243 cm^{-1}, 1192 cm^{-1}, 1133 cm^{-1}, 1088 cm^{-1}, 1063 cm^{-1} [48]. The out-plane C—H bending

Table 2
Optimized geometrical parameters of $Ag_2(NO_3)_2(C_8H_6IN)_2$ in comparison with experimental X-ray diffraction data.

Bond Lengths (Å)			Bond Angles (°)		
Parameter	6–311++g (d,p) with DGDZVP	XRD	Parameter	6–311++g (d,p) with DGDZVP	XRD
C_2–C_3	1.446	1.438 (7)	C_2–C_3–C_4	133.66	134.46 (5)
C_3–C_4	1.404	1.397 (7)	C_3–C_4–C_5	118.01	117.75 (4)
C_4–C_5	1.384	1.366 (7)	C_4–C_5–C_6	122.09	123.09 (5)
C_5–C_6	1.408	1.400 (7)	C_5–C_6–C_7	120.58	119.88 (5)
C_6–C_7	1.386	1.370 (7)	C_6–C_7–C_8	117.72	117.91 (5)
C_7–C_8	1.396	1.390 (7)	C_3–C_8–C_7	122.03	122.21 (5)
C_3–C_8	1.416	1.407 (7)	C_3–C_8–N_1	107.50	108.30 (5)
C_1–N_1	1.370	1.363 (7)	C_7–C_8–N_1	130.46	129.48 (5)
C_8–N_1	1.383	1.368 (6)	C_8–N_1–C_1	109.65	108.81 (4)
C_5–I_1	2.136	2.105 (5)	N_1–C_1–C_2	109.52	110.19 (5)
C_9–C_{10}	1.371	1.373 (8)	I_1–C_4–C_5	119.24	120.14 (4)
C_{10}–C_{11}	1.435	1.433 (7)	I_1–C_5–C_6	118.66	116.69 (4)
C_{11}–C_{12}	1.402	1.392 (7)	C_9–C_{10}–C_{11}	106.74	106.82 (5)
C_{12}–C_{13}	1.381	1.373 (7)	C_{10}–C_{11}–C_{12}	133.44	133.98 (5)
C_{13}–C_{14}	1.404	1.402 (8)	C_{11}–C_{12}–C_{13}	117.42	117.81 (5)
C_{14}–C_{15}	1.389	1.375 (9)	C_{12}–C_{13}–C_{14}	123.66	122.48 (5)
C_{15}–C_{16}	1.395	1.387 (7)	C_{13}–C_{14}–C_{15}	119.36	120.11 (5)
C_{11}–C_{16}	1.422	1.402 (7)	C_{14}–C_{15}–C_{16}	118.05	117.75 (5)
C_9–N_2	1.380	1.352 (7)	C_{11}–C_{16}–C_{15}	122.19	122.24 (5)
C_{16}–N_2	1.377	1.371 (7)	C_{11}–C_{16}–N_2	106.91	107.60 (4)
C_{13}–I_2	2.156	2.104 (5)	C_9–N_2–C_{16}	109.51	109.78 (5)
Ag_1–O_1	2.557	2.389 (5)	C_{15}–C_{16}–N_2	130.87	130.15 (5)
Ag_1–C_1	2.745	2.591 (5)	N_2–C_9–C_{10}	109.61	109.36 (5)
Ag_1–C_2	2.571	2.409 (5)	I_2–C_{13}–C_{14}	117.97	117.07 (4)
Ag_2–O_2	2.368	2.474 (5)	I_1–C_{13}–C_{12}	118.27	120.43 (4)
Ag_2–O_3	2.892	2.653 (5)	O_1–Ag_1–C_1	83.66	83.43 (17)
Ag_2–C_9	3.375	2.680 (6)	O_1–Ag_1–C_2	110.10	114.43 (17)
Ag_2–C_{10}	3.021	2.495 (5)	C_2–Ag_1–C_1	30.02	31.60 (18)
Ag_2–O_4	2.406	2.464 (4)	O_4–Ag_2–O_3	115.79	121.87 (16)
O_1–N_3	1.251	1.243 (6)	O_2–Ag_2–C_{10}	108.90	97.27 (17)
O_2–N_3	1.239	1.268 (6)	O_2–Ag_2–O_3	47.64	48.93 (14)
O_3–N_3	1.239	1.251 (6)	C_{10}–Ag_2–O_3	88.09	93.49 (17)
O_4–N_4	1.279	1.248 (6)	O_3–Ag_2–C_9	105.23	105.47 (17)
O_5–N_4	1.278	1.245 (6)	C_{10}–Ag_2–C_9	23.94	30.50 (18)
O_6–N_4	1.222	1.228 (6)	O_1–N_3–O_2	121.00	120.11 (5)
Ag_1–O_4^i	–	2.669 (4)	O_1–N_3–O_3	119.39	121.41 (5)
Ag_1–I_2^{ii}	–	2.749 (6)	O_2–N_3–O_3	119.59	118.46 (5)
Ag_2–I_1^{ii}	–	2.860 (6)	O_4–N_4–O_5	117.04	118.58 (5)
			O_4–N_4–O_6	121.46	120.87 (5)
			O_5–N_5–O_5	121.48	120.54 (5)
			C_2–Ag_1–O_4^i	–	85.47 (16)
			C_1–Ag_1–O_4^i	–	87.68 (16)
			O_1–Ag_1–I_2^{ii}	–	111.75 (11)
			C_2–Ag_1–I_2^{ii}	–	133.42 (14)
			C_1–Ag_1–I_2^{ii}	–	164.81 (13)
			O_4^i–Ag_1–I_2^{ii}	–	93.91 (10)
			O_4–Ag_2–I_1^{ii}	–	78.88 (11)
			O_2–Ag_2–I_1^{ii}	–	135.90 (11)
			O_1–Ag_1–O_4^i	–	83,71 (15)
			C_{10}–Ag_2–I_1^{ii}	–	109.05 (13)
			O_3–Ag_2– I_1^{ii}	–	93.64 (10)
			C_9–Ag_2–I_1^{ii}	–	134.43 (13)

Å:Angstrom, °: degree, Symmetry codes: (i) $-x+2, -y, -z+1$; (ii) $-x+2, -y+1, -z+1$.

vibrations of title molecule were experimentally observed at 754 (vs IR), 772 (m, Ra), 791 (vs IR), 860 (m, IR), 876 (m, IR)/ 876 (m,Ra), 901 (vw, IR), 946 (w, IR). Calculated values for out-plane C—H bending vibrations were found to be 752 cm^{-1}, 772 cm^{-1}, 798 cm^{-1}, 869 cm^{-1}, 876 cm^{-1}, 889 cm^{-1}, 898 cm^{-1}, 909 cm^{-1}, 911 cm^{-1}, 941 cm^{-1}, 963 cm^{-1}. These modes were observed at 754 cm^{-1} (vs IR), 772 cm^{-1} (m, Ra), 860 cm^{-1} (m,IR), 876 cm^{-1} (m, IR/ w, Ra) and 901 cm^{-1} (vw, IR). These modes for 5-iodoindole ligand were determined at 929 cm^{-1}, 884 cm^{-1}, 795 cm^{-1}, 760 cm^{-1}, and 728 cm^{-1} in the FT-IR spectrum and at 766 cm^{-1} in the FT-Ra spectrum, and also calculated at 949 cm^{-1}, 888 cm^{-1}, 866 cm^{-1}, 809 cm^{-1}, 771 cm^{-1}, and 729 cm^{-1} [48].

The C—C and C═C stretching vibrations for aromatic structure rings occur in the region of 1650 cm^{-1}-1200 cm^{-1} [48]. The C═C stretching vibrations were calculated at 1643 cm^{-1}, 1639 cm^{-1}, 1529 cm^{-1}, 1481 cm^{-1}, 1339 cm^{-1} and, 1330 cm^{-1}. Observed C═C stretching vibration modes for the title complex in the FT-IR and FT-Ra spectra are at 1330 cm^{-1} and 1332 cm^{-1}. Also, the C—C stretching vibrations were found at 1597 cm^{-1}, 1591 cm^{-1}, 1472 cm^{-1}, 1467 cm^{-1}, 1435 cm^{-1}, 1429 cm^{-1}, 1362 cm^{-1}, 1356 cm^{-1}, 1350 cm^{-1}, 1339 cm^{-1}, 1281 cm^{-1}, 1268 cm^{-1} and, 1206 cm^{-1}. These vibration modes were experimentally observed at 1603 cm^{-1} (vw, IR)/1615 cm^{-1} (m, Ra), 1561 cm^{-1} (w, IR)/1571 cm^{-1} (s, Ra), 1457 cm^{-1} (vw, Ra), 1445 cm^{-1} (m, IR)/1413 cm^{-1} (w, Ra), 1377 cm^{-1} (s, IR), 1287 cm^{-1} (vs IR), and 1191 cm^{-1} (s, IR/ vw, Ra). The C—C vibration peaks of 5-iodoindole were observed at 1621 cm^{-1}, 1406 cm^{-1}, 1309 cm^{-1} in the FT-IR spectrum and at 1408 cm^{-1} in the Raman spectrum, while the C═C stretching vibrations were

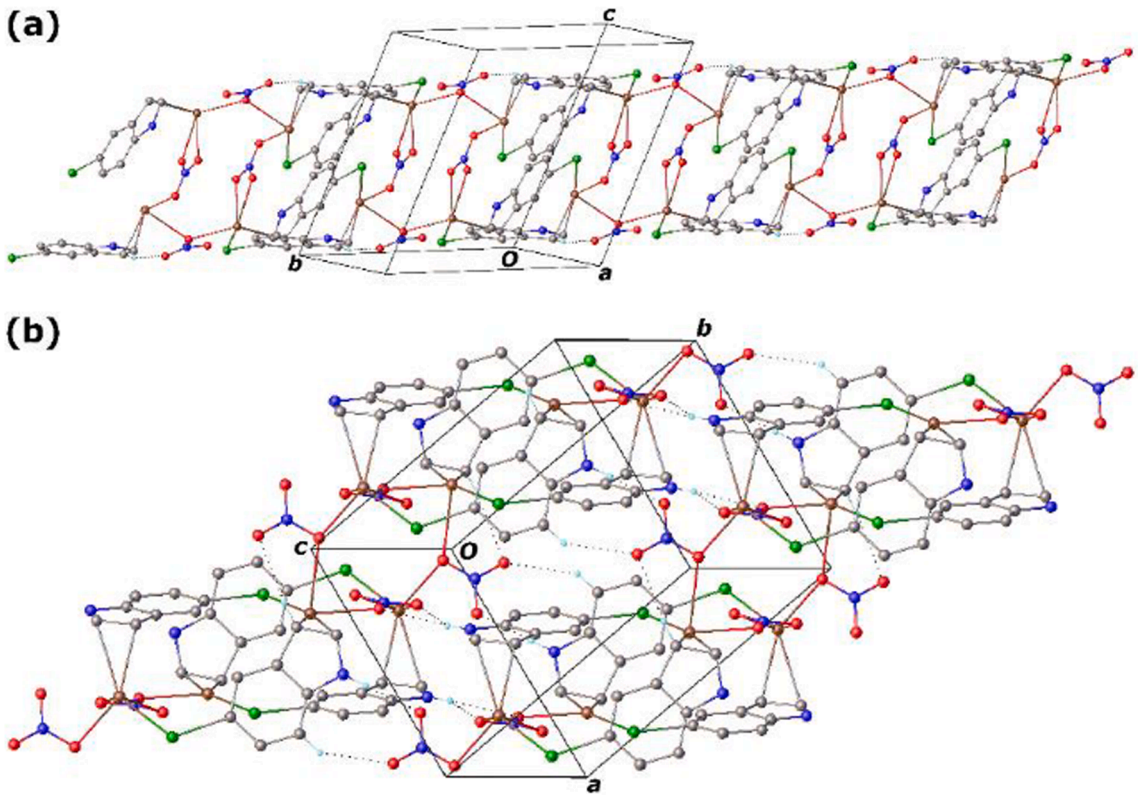

Fig. 2. **(a)** A one-dimensional coordination polymer of $Ag_2(NO_3)_2(C_8H_6IN)_2$ along the *b* axis and (**b**) Part of the crystal structure of $Ag_2(NO_3)_2(C_8H_6IN)_2$, showing the intermolecular interactions represented by dotted lines.

Table 3
Hydrogen bonding geometry for $Ag_2(NO_3)_2(C_8H_6IN)_2$.

D—H···A	D—H (Å)	H···A (Å)	D···A (Å)	D—H···A (°)
C2—H2···O6^{i}	0.93	2.55	3.464(7)	167
N1—H1N···O5^{iii}	0.86	2.09	2.930(6)	167
N2—H2N···O1^{iii}	0.86	2.38	3.192(7)	157
C7—H7···O6^{iii}	0.93	2.52	3.334(7)	146
N2—H2N···O2^{iii}	0.86	2.22	2.963(6)	145

Symmetry codes: (i) − x + 2, −y, −z + 1; (iii) − x + 1, −y, −z + 1.

determined at 1589 cm^{-1}, 1461 cm^{-1}, 1438 cm^{-1}, 1332 cm^{-1} in the FT-IR spectrum and 1500 cm^{-1} and 1443 cm^{-1} in the FT-Ra spectrum. Also these vibration values for 5-iodoindole were calculated at 1640 cm^{-1}, 1434 cm^{-1}, 1331 cm^{-1} for the C—C stretching vibrations and at 1594 cm^{-1}, 1480 cm^{-1}, 1474 cm^{-1}, 1366 cm^{-1} for the C=C stretching modes [48].

The C—N stretching vibrations are observed in the region of 1342 cm^{-1}-1266 cm^{-1} [51], but the identification of these vibrations is very difficult since they are superimposed with the other vibrations such as the C—C stretching, CCH and CNH bending in this region [52]. The C—N stretching modes were calculated at 1092 cm^{-1} and observed at 1091 cm^{-1} (m, IR) in the FT-IR spectrum. This mode for the free 5-iodoindole molecule was observed at 1088 cm^{-1} and calculated at 1434 cm^{-1} and 1108 cm^{-1} [48].

While the N—O stretching modes of the nitrate group of $Ag_2(NO_3)_2(C_8H_6IN)_2$ complex were observed at 1377 cm^{-1} (s, IR), 1236 cm^{-1} (s, IR), 1250 cm^{-1} (m, Ra), 1072 cm^{-1} (w, Ra), 1036 cm^{-1} (m, IR), and 1045 cm^{-1} (vw, Ra) in the FT-IR and FT-Ra spectra. These modes were calculated at 1511 cm^{-1}, 1350 cm^{-1}, 1265 cm^{-1}, 1070 cm^{-1}, and 1046 cm^{-1}. In addition, some N—O and Ag-O stretching vibrations were observed together at 727 cm^{-1} (vs IR), and were calculated at 725 cm^{-1} and 705 cm^{-1}. The other Ag-O stretching vibrations were theoretically found to be 226 cm^{-1}, 180 cm^{-1}, 153 cm^{-1}, 127 cm^{-1}, and 122 cm^{-1} and were experimentally observed at 121 cm^{-1} (vs Ra).

In the literature, Ag(I)-O stretching vibration of [Ag(3-PyCHO)$_2$(NO$_3$)] complex in IR spectrum was given a medium peak at 642 cm^{-1} and were calculated at 650 cm^{-1}, 648 cm^{-1}, and 180 cm^{-1} [20]. In the other study, [Ag(methyl 4-pyridyl ketone)]$_2$NO$_3$ compound exhibited N—O stretching modes at 1499 cm^{-1}, 1063 cm^{-1}, and 689 cm^{-1} in the IR spectrum and at 1071 cm^{-1} in the Raman spectrum and these modes were calculated at 1502 cm^{-1}, 1058 cm^{-1}, and 728 cm^{-1} [53]. Ag-O stretching vibration for $(C_{10}H_9N_3)AgNO_3$ complex was observed at 232 (IR) cm^{-1}calculated at 243 cm^{-1}. Also, N—O stretching vibrations in the same study were observed 953 cm^{-1} (IR), 1099 cm^{-1} (IR), and 1110 cm^{-1} (Ra) and were calculated 911 cm^{-1} and 1135 cm^{-1} [54].

For the title complex, the Ag-C stretching vibration was calculated at 134 cm^{-1} and was observed 137 cm^{-1} as a very weak band. In the literature, it has been stated that in the frequency region 400–155 cm^{-1}, the stretching Ag-C, Ag-S, and Ag-N vibrations have been expected. For [Ag(Tu)(CN)], $[Ag(Dmtu)_2]^+[Ag(CN)_2]^-$, and $[Ag(Imt)_2]^+[Ag(CN)_2]^-$ structures, Ag-C stretching vibrations were calculated at 338 cm^{-1}, 393 cm^{-1} and 393 cm^{-1}, respectively [55]. In the study named "Ethylene and oxygen species adsorbed on defect oxidized surface Ag(1 1 1) theoretical analysis by DFT method" by Avdeev and Zhidomirov, symmetric and antisymmetric Ag-C stretching vibrations were obtained at 169 cm^{-1} and 179 cm^{-1} for Ag-CH_2-Ag [56]. Also, in the study called Surface-enhanced Raman spectroscopy of CO adsorbed on colloidal silver particles, strong Ag-C tension vibration was observed at 169 cm^{-1} [57]. In another study, Ag-C stretching vibration was reported at 350 cm^{-1} for $(CH_3)_4NAg(CN)_2$ complex and at 367 cm^{-1} for $(C_6H_5)_4AsAg(CN)_2$ complex [58].

When the previous study of 5-iodoindole ligand and this study prepared for silver nitrate complex structure were compared, according to the experimental IR and Raman spectra for both structures, new vibration peaks were observed at 122 cm^{-1} (IR)/121 cm^{-1} (Ra), 137 cm^{-1}

Table 4
Calculated vibrational wavenumbers, frequencies, scaled frequencies, normalized absorption intensities of infrared and Raman spectra and observed infrared and Raman frequencies, and their detailed assignments with total energy distribution (%) for $Ag_2(NO_3)_2(C_8H_6IN)_2$.

Calculated					Observed		
Mode	Fre	Fre[a]	I_{IR}[b]	I_{RA}[b]	IR	Raman	% TED[c]
1	6	6	0.12	86.20	–	–	$14\Gamma_{IAgCC} + 14\Gamma_{OAgCC} + 10\Gamma_{OAgCH}$
2	7	7	0.10	27.05	–	–	$14\Gamma_{IAgCC} + 14\Gamma_{OAgON}$
3	12	12	0.15	100.00	–	–	$14\Gamma_{AgICC} + 10\Gamma_{OAgON}$
4	15	15	0.01	33.18	–	–	$15\Gamma_{OAgON}$
5	17	17	0.42	9.46	–	–	$16\Gamma_{OAgON}$
6	21	21	0.42	7.57	–	–	$21\Gamma_{IAgCC} + 10\Gamma_{OAgON}$
7	25	25	0.05	10.63	–	–	$13\Gamma_{OAgON}$
8	30	30	1.09	2.31	–	–	$37\Gamma_{OAgON}$
9	33	33	0.18	0.64	–	–	$33\Gamma_{OAgON}$
10	36	36	0.32	12.29	–	–	$16\Gamma_{OAgON}$
11	44	44	0.45	3.54	–	–	$12\delta_{OAgO} + 29\Gamma_{OAgON}$
12	48	48	0.31	2.99	50vw	–	$10\delta_{OAgO} + 30\Gamma_{OAgON}$
13	58	57	0.16	4.70	–	–	$10\Gamma_{IAgCC}$
14	62	62	0.04	7.26	62 *m*	–	$10\Gamma_{IAgCC} + 16\Gamma_{OAgON}$
15	88	88	0.95	0.97	–	–	$14\Gamma_{AgONO}$
16	95	95	0.02	2.11	–	–	$17\Gamma_{AgONO}$
17	101	101	1.13	0.52	–	–	$11\Gamma_{CCCC} + 11\Gamma_{AgONO}$
18	105	105	0.91	1.20	106 *m*	–	$10\Gamma_{CCCC} + 10\Gamma_{CCCI}$
19	112	111	0.86	1.56	–	–	$13\Gamma_{OAgON} + 32\Gamma_{AgONO}$
20	118	118	0.46	0.56	–	–	$17\Gamma_{OAgON} + 24\Gamma_{AgONO}$
21	122	122	0.57	0.33	122 *m*	121vs	$22\upsilon_{AgO} + 27\Gamma_{OAgON} + 36\Gamma_{AgONO}$
22	127	127	0.13	0.06	–	–	$22\upsilon_{AgO} + 17\Gamma_{OAgON} + 20\Gamma_{AgONO}$
23	134	134	1.04	2.05	137w	–	$12\upsilon_{AgC} + 13\Gamma_{CCCC} + 10\Gamma_{CCCH}$
24	154	154	1.79	0.10	–	–	$33\upsilon_{AgO} + 15\Gamma_{OAgON}$
25	168	168	0.08	0.38	–	–	$18\delta_{CCI}$
26	170	170	0.19	0.28	–	–	$14\delta_{CCI}$
27	180	179	2.85	0.04	–	–	$33\upsilon_{AgO} + 10\Gamma_{OAgON}$
28	225	225	1.48	0.80	–	–	$23\upsilon_{AgO} + 12\Gamma_{CCCC}$
29	227	226	6.88	0.11	–	–	$19\upsilon_{AgO} + 17\Gamma_{CCCC}$
30	233	232	0.09	0.67	239vw	231w	$17\upsilon_{IC} + 15\delta_{CCC}$
31	234	233	2.25	0.05	–	–	$24\Gamma_{CCCC} + 14\Gamma_{CCCH} + 10\Gamma_{CNCC}$
32	256	255	0.16	0.06	–	–	$21\Gamma_{CCCC} + 16\Gamma_{CCCH}$
33	301	301	0.16	0.03	–	–	$23\Gamma_{CCCC} + 15\Gamma_{CCCH} + 13\Gamma_{CNCC}$
34	309	309	0.95	0.09	–	–	$23\Gamma_{CCCC} + 13\Gamma_{CCCH} + 17\Gamma_{CNCC}$
35	420	419	2.07	0.01	411 *m*	–	$27\Gamma_{CCCC} + 24\Gamma_{CCCH}$
36	422	420	0.62	0.01	–	–	$18\Gamma_{CCCC} + 16\Gamma_{CCCH}$
37	426	425	0.90	0.03	–	–	$14\delta_{CCC} + 23\Gamma_{CCCC} + 18\Gamma_{CCCH}$
38	428	426	1.99	0.02	–	–	$25\Gamma_{CCCC} + 23\Gamma_{CCCH}$
39	449	448	11.07	0.03	–	–	$41\Gamma_{CCNH} + 15\Gamma_{HNCH}$
40	499	498	17.24	0.05	494 *m*	–	$43\Gamma_{CCNH} + 14\Gamma_{HNCH}$
41	573	571	0.73	0.05	561 *m*	–	$25\delta_{CCC} + 21\delta_{CCH}$
42	578	576	0.40	0.06	–	572vw	$21\delta_{CCC} + 19\delta_{CCH}$
43	584	582	1.51	0.03	582 *m*	–	$22\Gamma_{CCCC} + 31\Gamma_{CCCH}$
44	594	592	1.61	0.02	595 s	–	$25\Gamma_{CCCC} + 24\Gamma_{CCCH}$
45	615	613	0.24	0.01	614vw	–	$10\Gamma_{CCCC} + 14\Gamma_{CCCH} + 10\Gamma_{CNCC} + 12\Gamma_{CCNH}$
46	623	621	0.01	0.05	–	–	$20\Gamma_{CCCC} + 18\Gamma_{CCCH}$
47	655	653	2.64	0.12	648vs	647vw	$10\upsilon_{IC} + 28\delta_{CCC} + 11\delta_{CCH}$
48	663	661	2.21	0.13	–	–	$25\delta_{CCC} + 10\delta_{CCH}$
49	707	705	0.04	0.02	–	–	$22\upsilon_{AgO} + 15\upsilon_{NO} + 34\delta_{ONO}$
50	727	725	3.07	0.02	727vs	–	$19\upsilon_{AgO} + 10\upsilon_{NO} + 34\delta_{ONO} + 11\delta_{AgON}$
51	739	737	0.69	0.02	–	–	$27\Gamma_{CCCC} + 25\Gamma_{CCCH}$
52	741	739	0.65	0.02	–	–	$12\delta_{ONO} + 15\Gamma_{CCCC} + 17\Gamma_{CCCH}$
53	742	740	0.43	0.04	–	–	$11\upsilon_{AgO} + 12\delta_{ONO} + 20\Gamma_{CCCC} + 17\Gamma_{CCCH}$
54	754	752	1.83	0.01	754vs	–	$27\Gamma_{CCCC} + 19\Gamma_{CCCH}$
55	775	772	15.20	0.03	–	772 *m*	$36\Gamma_{CCCH} + 10\Gamma_{NCCH}$
56	782	779	5.90	0.14	–	–	$10\Gamma_{CCCC} + 26\Gamma_{CCCH}$
57	785	783	11.73	0.57	–	–	$24\Gamma_{CCCH}$
58	787	784	0.39	0.42	–	–	$14\upsilon_{CC} + 16\delta_{CCC} + 10\delta_{CCH} + 14\Gamma_{CCCH}$
59	800	798	1.90	0.02	791vs	–	$17\Gamma_{CCCC} + 35\Gamma_{CCCH} + 12\Gamma_{NCCH} + 10\Gamma_{ICCH}$
60	815	813	4.22	0.01	–	–	$15\Gamma_{CCCC} + 36\Gamma_{CCCH} + 12\Gamma_{NCCH} + 10\Gamma_{ICCH}$
61	820	817	1.10	0.00	–	–	$45\Gamma_{AgONO} + 17\Gamma_{OAgON}$
62	823	821	1.62	0.00	–	–	$54\Gamma_{AgONO} + 33\Gamma_{OAgON}$
63	872	869	2.47	0.19	860 *m*	–	$22\Gamma_{CCCH} + 123\Gamma_{HCCH}$
64	879	876	5.26	0.19	876 *m*	876w	$13\gamma_{CCC} + 10\gamma_{CCH} + 19\Gamma_{CCCH}$
65	886	883	2.03	0.03	–	–	$10\Gamma_{CCCC} + 36\Gamma_{CCCH} + 11\Gamma_{HCCH}$
66	892	889	5.83	0.21	–	–	$12\gamma_{CCC} + 10\gamma_{CCH} + 15\Gamma_{CCCH}$
67	898	895	2.28	0.03	–	–	$35\Gamma_{CCCH} + 12\Gamma_{HCCH}$
68	901	898	2.55	0.01	901vw	–	$14\Gamma_{CCCC} + 39\Gamma_{CCCH} + 12\Gamma_{ICCH}$
69	912	909	0.49	0.08	–	–	$10\gamma_{CCC} + 16\gamma_{CCH} + 12\Gamma_{CCCH}$
70	913	911	0.60	0.04	–	–	$11\gamma_{CCH} + 14\Gamma_{CCCH}$

(*continued on next page*)

Table 4 (*continued*)

Calculated					Observed		
Mode	**Fre**	**Fre**[a]	**I_{IR}**[b]	**I_{RA}**[b]	**IR**	**Raman**	**% TED**[c]
71	944	941	0.10	0.00	946w	–	$11\Gamma_{CCCC} + 37\Gamma_{CCCH} + 10\Gamma_{NCCH} + 18\Gamma_{HCCH} + 10\Gamma_{ICCH}$
72	966	963	0.04	0.00	–	–	$12\Gamma_{CCCC} + 46\Gamma_{CCCH} + 19\Gamma_{HCCH} + 10\Gamma_{ICCH}$
73	1049	1046	7.94	0.31	1036 *m*	1045vw	$48\upsilon_{NO} + 14\delta_{OAgO} + 10\delta_{ONO} + 12\Gamma_{OAgON}$
74	1057	1054	0.70	0.22	–	–	$22\upsilon_{CC} + 22\delta_{CCC} + 27\delta_{CCH}$
75	1064	1061	1.50	0.26	1057 *m*		$22\upsilon_{CC} + 13\delta_{CCC} + 34\delta_{CCH}$
76	1073	1070	0.59	0.30	–	1072w	$23\upsilon_{NO} + 11\Gamma_{OAgON}$
77	1083	1079	1.06	0.53	–	–	$27\delta_{CCH} + 10\Gamma_{IAgCH}$
78	1095	1092	0.86	0.25	1091 *m*	–	$12\upsilon_{CC} + 11\upsilon_{CN} + 40\delta_{CCH} + 11\delta_{CNH}$
79	1115	1111	5.65	0.04	–	–	$14\delta_{CCC} + 42\delta_{CCH} + 12\delta_{CNH} + 12\delta_{NCH}$
80	1127	1124	4.96	0.01	1135 *m*	1131vw	$12\delta_{CCC} + 18\delta_{CCH} + 10\delta_{CNH}$
81	1157	1154	0.67	0.02	–	–	$15\upsilon_{CC} + 13\delta_{CCC} + 47\delta_{CCH}$
82	1163	1160	0.19	0.03	–	–	$12\upsilon_{CC} + 10\delta_{CCC} + 38\delta_{CCH}$
83	1209	1206	1.30	0.04	1191 s	1191vw	$14\upsilon_{CC} + 15\delta_{CCC} + 33\delta_{CCH}$
84	1209	1206	1.09	0.06	–	–	$14\upsilon_{CC} + 17\delta_{CCC} + 27\delta_{CCH}$
85	1267	1263	1.53	0.26	–	–	$10\upsilon_{CC} + 39\delta_{CCH}$
86	1269	1265	36.06	0.04	1236 s	1250 *m*	$17\upsilon_{NO} + 31\delta_{CCH} + 11\delta_{ONO}$
87	1271	1268	7.62	0.09	–	–	$10\upsilon_{CC} + 11\upsilon_{NO} + 37\delta_{CCH}$
88	1277	1273	1.37	0.35	–	–	$18\upsilon_{CC} + 25\delta_{CCH}$
89	1285	1281	1.89	0.16	1287vs	–	$19\upsilon_{CC} + 10\delta_{CCC} + 29\delta_{CCH} + 13\delta_{CNH}$
90	1334	1330	5.11	0.12	1330 s	1332 s	$25\upsilon_{CC} + 28\delta_{CCH}$
91	1343	1339	6.59	0.10	–	–	$28\upsilon_{CC} + 29\delta_{CCH}$
92	1355	1350	40.17	0.01	1377 s	–	$23\upsilon_{NO} + 10\upsilon_{CC} + 16\delta_{CCH} + 33\delta_{ONO}$
93	1360	1356	1.35	0.62	–	–	$21\upsilon_{CC} + 33\delta_{CCH}$
94	1366	1362	0.97	0.27	–	–	$26\upsilon_{CC} + 44\delta_{CCH}$
95	1431	1427	12.54	0.30	–	–	$14\upsilon_{CC} + 25\delta_{CCH} + 10\delta_{CNH}$
96	1434	1429	100.00	0.07	1445 *m*	1413w	$11\upsilon_{CC} + 29\delta_{CCH} + 10\delta_{ONO}$
97	1439	1435	10.99	0.19	–	–	$18\upsilon_{CC} + 27\delta_{CCH} + 14\delta_{CNH}$
98	1472	1467	7.40	0.21	–	1457vw	$24\upsilon_{CC} + 36\delta_{CCH}$
99	1477	1472	3.56	0.23	–	–	$20\upsilon_{CC} + 37\delta_{CCH}$
100	1484	1480	4.88	0.23	–	–	$19\upsilon_{CC} + 12\delta_{CCC} + 21\delta_{CCH}$
101	1486	1481	8.52	0.10	–	–	$20\upsilon_{CC} + 16\delta_{CCC} + 21\delta_{CCH} + 14\delta_{CNH}$
102	1515	1510	10.64	0.97	–	–	$14\upsilon_{CC} + 30\delta_{CCH}$
103	1516	1511	94.93	0.09	–	–	$30\upsilon_{NO} + 13\delta_{CCH} + 16\delta_{ONO}$
104	1534	1529	1.26	0.75	–	–	$20\upsilon_{CC} + 12\delta_{CCC} + 33\delta_{CCH}$
105	1596	1591	2.02	0.06	1561w	1571 s	$30\upsilon_{CC} + 14\delta_{CCC} + 29\delta_{CCH}$
106	1602	1597	2.72	0.10	1603vw	1615 *m*	$27\upsilon_{CC} + 14\delta_{CCC} + 22\delta_{CCH}$
107	1644	1639	0.26	0.13	–	–	$29\upsilon_{CC} + 16\upsilon_{CCC} + 22\delta_{CCH}$
108	1648	1643	0.28	0.07	–	–	$29\upsilon_{CC} + 16\delta_{CCC} + 24\delta_{CCH}$
109	3180	3037	0.72	0.14	2956vw	–	$76\ \upsilon_{CH}$
110	3184	3041	0.39	0.10	–	–	$75\ \upsilon_{CH}$
111	3198	3054	0.05	0.04	–	–	$70\upsilon_{CH}$
112	3208	3063	0.00	0.02	–	–	$74\ \upsilon_{CH}$
113	3209	3064	0.23	0.13	–	–	$77\ \upsilon_{CH}$
114	3210	3065	0.29	0.11	–	3069 *m*	$79\ \upsilon_{CH}$
115	3226	3081	0.40	0.06	–	–	$64\ \upsilon_{CH}$
116	3240	3095	0.38	0.05	–	–	$77\ \upsilon_{CH}$
117	3252	3106	0.55	0.10	3102w	3112w	$71\ \upsilon_{CH}$
118	3263	3116	0.95	0.15	–		$77\ \upsilon_{CH}$
119	3648	3484	15.19	0.08	3280w	3340vw	$73\ \upsilon_{NH}$
120	3664	3499	15.74	0.11	3412w	3411 s	$76\ \upsilon_{NH}$

υ: stretching, δ: in-plane bending, γ out-plane bending vibration, Γ: torsion; s: strong, m: medium, w: weak, v: very.

[a] Scaled wavenumbers calculated at Density Functional Theory/Becke three Lee-Yang-Parr/6–311++G(d,p) with DGDZVP using scaling factors 0.997 for the wavenumber less than 1800 cm^{-1} and 0.955 above 1800 cm^{-1} [48].

[b] Relative absorption intensities and relative Raman intensities normalized with highest peak absorption equal to 100.

[c] Total energy distribution (TED) calculated Density Functional Theory/Becke three Lee-Yang-Parr/6–311++G(d,p) with DGDZVP level, TED less than 10 % are not shown.

(Ir), 1036 cm^{-1} (Ir)/1045 cm^{-1} (Ra), 1072 cm^{-1} (Ra), and 1377 cm^{-1} (Ir). Therefore, we can say that the complex has acquired a new characteristic feature.

3.4. ^1H NMR analysis

One of the important techniques used in the structural analysis of organic molecules is chemical shift analysis [59]. Experimental and theoretical ^1H NMR analysis was performed to obtain information about the number of protons in the title molecule and the immediate environment of each of them. ^1H chemical shift values were calculated in chloroform solvent by using Gauge Independent Atomic Orbital (GIAO) at DFT (B3LYP method)/6–311++G(2d,p) with DGDZVP over the optimized structure. The ^1H NMR spectrum of the title complex structure was recorded with chemical shifts in the range of 0–15 ppm. Analysis results are given in Table 5 and presented in Fig. 4. The experimental chemical shift values of the complex were observed as follow: ^1H NMR (300 MHz, d-CDCl3) δ/ppm: 8.05 (H_{1N}), 8.20 (H_{2N}), 7.86 (H_1), 6.48 (H_2), 7.99 (H_4), 7.73 (H_6), 7.20 (H_7), 7.20 (H_9), 6.48 (H_{10}), 7.92 (H_{12}), 7.19 (H_{14}), and 7.45 (H_{15}). Also, the theoretical values corresponding to the experimental data were calculated as follows: 8.15, 8.20, 7.87, 9.90, 8.4, 7.33, 7.67, 7.69, 6.97, 7.78, 7.28, and 7.50 ppm, respectively. The values observed in the range of 1–5-2 ppm in the experimental data belong to the H_2O peaks in the solvent [60,61]. Both the experimental and theoretical values are in the standard value ranges (6.50–8.50 ppm) for H atoms, and they are also in good agreement with

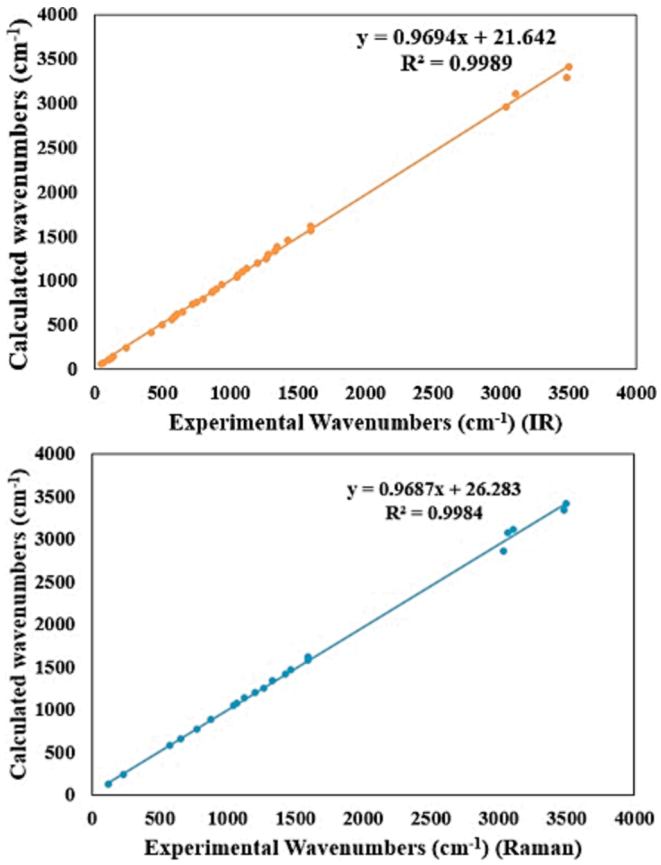

Fig. 3. Correlation graphics between theoretical and experimental wavenumbers (cm^{-1}) of $Ag_2(NO_3)_2(C_8H_6IN)_2$.

Table 5
^1H NMR Chemical shift values of $Ag_2(NO_3)_2(C_8H_6IN)_2$.

Atom position	Calculated Values (ppm)	Experimental Values (ppm)
H_{1N}	8.15	8.05
H_{2N}	8.20	8.20
H_1	7.87	7.86
H_2	9.90	6.48
H_4	8.40	7.99
H_6	7.33	7.73
H_7	7.67	7.20
H_9	7.69	7.20
H_{10}	6.97	6.48
H_{12}	7.78	7.92
H_{14}	7.28	7.19
H_{15}	7.50	7.45

each other.

3.5. Homo-Lumo analysis

The energies of the highest energy molecular orbital HOMO and the lowest energy molecular orbital LUMO are important parameters in quantum chemistry [62]. These two parameter values affect the electronic structure, charge transfer, chemical reactivity, optical properties, and dynamic stability of any chemical system. Also, molecular orbital theory is an important parameter used to understand biological properties such as antibacterial, DNA binding and antioxidant activity [63]. Chemical hardness, chemical potential, optical polarizability, chemical softness, and electrophilicity values are calculated from the HOMO and LUMO energy values using the following formulas:$I = -E_{HOMO}$,$A = -E_{LUMO}$,$\eta = (-E_{HOMO} + E_{LUMO})/2$,$\mu_c = (E_{HOMO} + E_{LUMO})/2$, $\chi = -\mu_c$ and $\omega = \mu_c^2/2\eta$[64,65]. The HOMO and LUMO energies, the associated energy gap, and the other properties energy values have been calculated at B3LYP/6–311++G(d,p) with DGDZVP basis set in the gas phase and are listed Table 6.

If the energy values of the HOMO and LUMO molecular orbitals are excessive, the complexes can more easily release electrons towards biological materials. When the biological reactivity increases with the rise of the energy value of HOMO and the energy value of LUMO decreases, the molecular electron biological activity increases. [20]. Also, hard materials with low chemical reactivity have a large energy gap, while soft materials with high chemical reactivity have a small energy gap. The HOMO and LUMO energy values are −5.98 eV and −2.18 eV, respectively. The HOMO-LUMO energy gap value of title molecule is 3.80 eV. Also, the values of ionization potential (I), electron affinity (A), global hardness (η), electronegativity (χ), chemical potential (μ_c), global softness (σ), global electrophilicity (ω) were found as follows: 5.98 eV, 2.18 eV, 1.90 eV, 4.07 eV, −4.07, 0.52, and 4.36 eV. When examined in the studies in the literature, the energy gap, global hardness and global softness values show that the title molecule has a hard structure and low reactivity [64,66,67]. In the other study, the energy gap of the free 5-iodoindole ligand was found to be 5.08 eV for the same basis set calculation [48]. The energy gap of the complex with silver nitrate of 5-iodoindole was found to be smaller than that of 5-iodoindole. Therefore, we can say that the complex structure is more reactive and softer than the free ligand.

The HOMO-LUMO distributions are given in Fig. 5. The positive and negative sites of $Ag_2(NO_3)_2(C_8H_6IN)_2$ are determined by red and green colors respectively. While the HOMO is distributed over the Ag_2 metal ion, N_4, O_4, O_5, and O_6 atoms (nitrate group), the LUMO is distributed over the C_{12}, C_{13}, C_{14}, C_{15}, and I_2 atoms.

The simulated density of state spectrum (DOS) that calculated by the Mulliken population shows in Fig. 6. This spectrum was created by combining current molecular energy levels with Gaussian curves of unit height. DOS is related to states of molecular orbitals at different energy levels of the molecule. The green and red lines in the spectrum allow to detected occupied and virtual orbitals more easily [68].

3.6. Hirshfeld surface analysis

To investigate the contributions of different intermolecular interactions in the crystal packing motif, Hirshfeld surface analysis and related two-dimensional fingerprint drawings were performed with CrystalExplorer 17 Software [33]. Hirshfeld surface analysis maps prepared according to d_{norm}, di, and de properties are shown in Fig. 7. d_e and d_i are the distances from a given point on the surface to the nearest atom outside and inside. The Hirshfeld surfaces mapped over the d_{norm} use the function of these normalized distances. The red, white, and blue colors used for d_{norm}-mapped Hirshfeld surfaces indicate short contacts, intermolecular distances equal to van der Waals radii, and longer contacts, [69–71].

According to d_{norm} Hirshfeld map, the red area corresponds to the more dominant interactions between oxygen and hydrogen atoms, while other visible spots on the Hirshfeld surface correspond to C—H, H—H, or I–H contacts. Looking at the Fig. 8 fingerprint plots, the O···H/H···O (27.7 %) interactions make the largest contribution to the Hirshfeld surfaces and are represented by the blue spikes on the lower left and right. C···H/H···C (15 %) interactions are above the O—H regions. The H···H contacts contribute 17 % to the Hirshfeld surfaces, while the I···H/H···I interactions contribute 10.2 % above the C—H regions.

3.7. Molecular electrostatic potential (MEP)

MEP is an electrostatic potential surface plot related to electron density [72]. It is one of the most important tools used to predict the chemical reactivity of molecules and ensure information about the

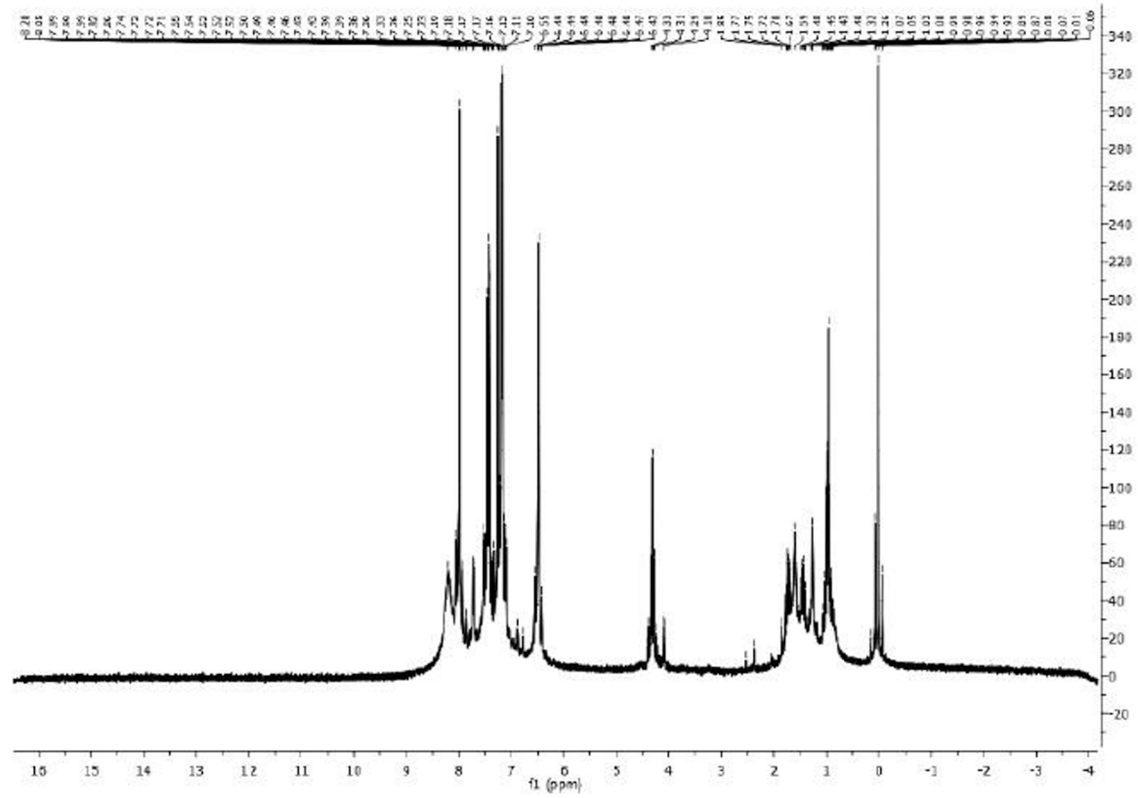

(a)

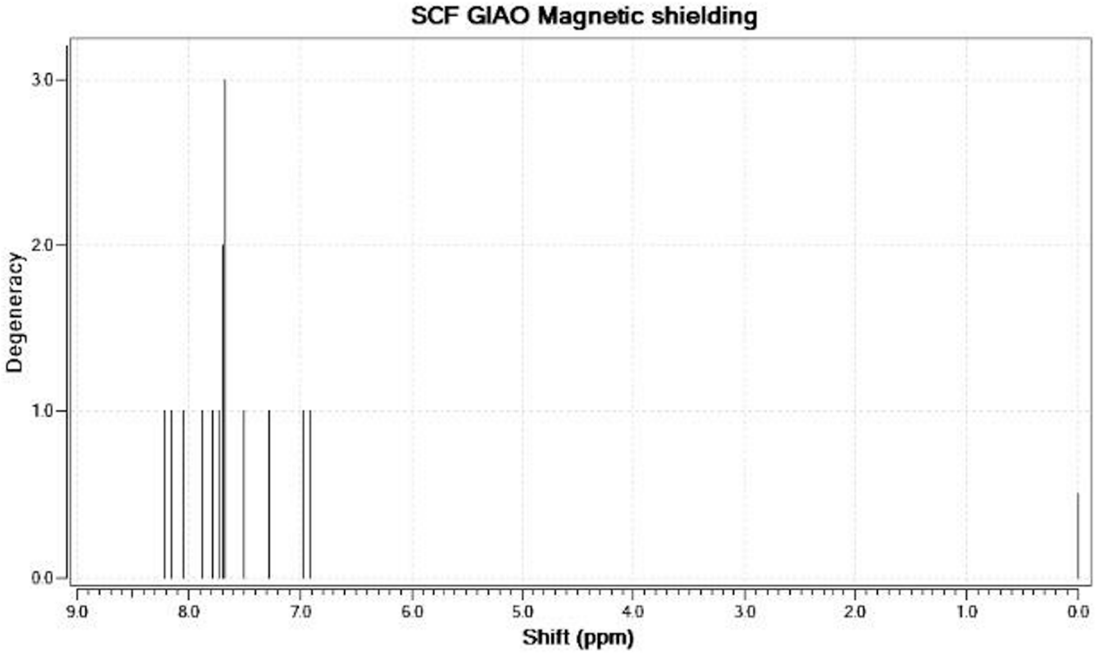

(b)

Fig. 4. Experimental (a) and theoretical (b) ^{1}H NMR spectra of $Ag_2(NO_3)_2(C_8H_6IN)_2$.

electrophilic and nucleophilic regions of the molecule with different color codes [73]. The order of the color scheme for the MEP from electron rich region to electron poor region is as follows: red (electron rich region) < yellow (slightly electron rich region) < green (neutral region/zero potential) < blue (electron deficient region/positive charges) [74].

The molecular electrostatic surface map for $Ag_2(NO_3)_2(C_8H_6IN)_2$ is shown in Fig. 9. The negative regions (electrophilic) of the title complex structure are particularly localized on the O_4, O_5, and O_6 atoms. Besides, O_1, O_2, and O_3 atoms with C_{10}, C_{11}, and C_{12} atoms in benzene and

Table 6
The calculated energy gaps and quantum chemical properties of title compound.

Molecular Orbitals	E (eV)		E_g (eV)	I (eV)	A (eV)	η(eV)	χ(eV)	μ_c(eV)	σ(eV)$^{-1}$	ω(eV)
H	−5.98	ΔE_{H-L}	3.80	5.98	2.18	1.90	4.07	−4.07	0.52	4.36
L	−2.18									
H-1	−6.47	$\Delta E_{H_{-1}-L_{+1}}$	4.52	6.47	1.96	2.26	4.21	−4.21	0.44	3.93
L + 1	−1.96									
H-2	−6.89	$\Delta E_{H_{-2}-L_{+2}}$	5.02	6.89	1.87	2.51	4.38	−4.38	0.39	3.82
L + 2	−1.87									

H: HOMO (Highest Occupied Molecular Orbital), L: LUMO (Lowest Unoccupied molecular orbital), eV: electron volt, (eV)$^{-1}$: 1/electron volt, E_g: Energy gap, I: Iozination potantial, A: electron affinity, η: global hardnes, χ: electronegativity, μ_c: chemical potential, σ: global softnes, ω: global electrophilicity.

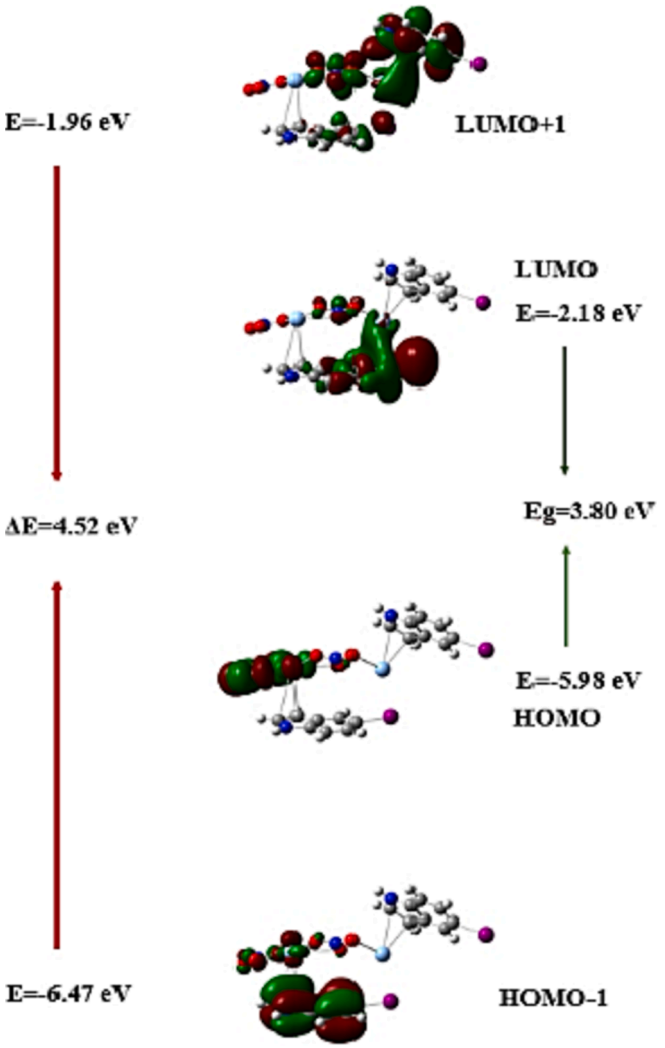

Fig. 5. Frontier molecular orbital diagrams of $Ag_2(NO_3)_2(C_8H_6IN)_2$ to determine the energy gap between molecular orbitals.

pyrrole rings are in slightly electron-rich regions. Ag_1 and Ag_2 atoms are in the electron-deficient light blue region. According to the electrostatic potential surface map, N_1 and N_2 atoms are also in the positive charges dark blue regions (nücleophilic). Also, a two-dimensional contour map of the title molecule is given in Fig. 10. This map again shows that the electron-rich regions are localized around the O atoms in the nitrate groups.

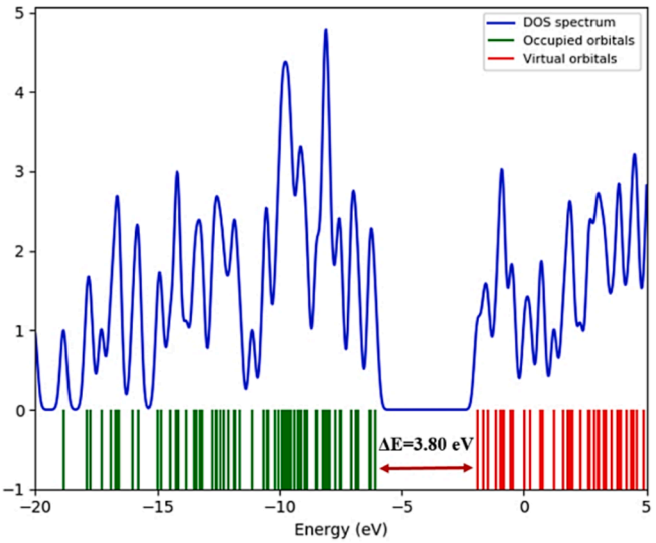

Fig. 6. The simulated density of states spectrum of $Ag_2(NO_3)_2(C_8H_6IN)_2$.

3.8. Charge analysis

The electronic charges of atoms, which affect the molecular moment, molecular parity, electronic structure and many other properties, provide important information about the binding potential of a molecule. Therefore, they have a very important function in quantum chemical computation studies [53,75,76]. The atomic charge analysis of the optimized structure was obtained by Natural Bond Orbital, Atomic Polar Tensor, and Hirshfeld charges. For atomic charge calculations of $Ag_2(NO_3)_2(C_8H_6IN)_2$, the 6–311++G (d, p) basis set was used for light atoms and the DGDZVP basis set was used for heavy atoms. The results are given in Table 7 and presented in supplementary Fig. S3.

According to the results obtained, all of the oxygen atoms in the nitrate groups of the structure were found to be the most negative compared to the other atoms. The N_3 and N_4 atoms in the nitrate group have a positive charge, while the N_1 and N_2 atoms in the pyrrole ring of 5-iodoindole have a negative charge. Ag_1 and Ag_2 silver metals are the most positive charged atoms. Iodine atoms were found to be negative in APT and Hirshfeld atomic charge analysis and positive in NBO charge analyses. The C_2, C_4, C_6, C_{10}, C_{12}, and C_{14} atoms of 5-iodoindole ligands in the complex structure were found to be negative in all three analysis methods. All H atoms have positive values. When the results obtained from the charge analysis of the title molecule are compared with the molecular electrostatic surface map, the electrophilic and nucleophilic regions in the MEP map are in good agreement with the charge analysis results.

In the charge analysis study conducted using the same basis set on the free ligand of 5-iodoindole, it was found that the N atom in the pyrrole ring of the ligand was the most negative atom, while some C

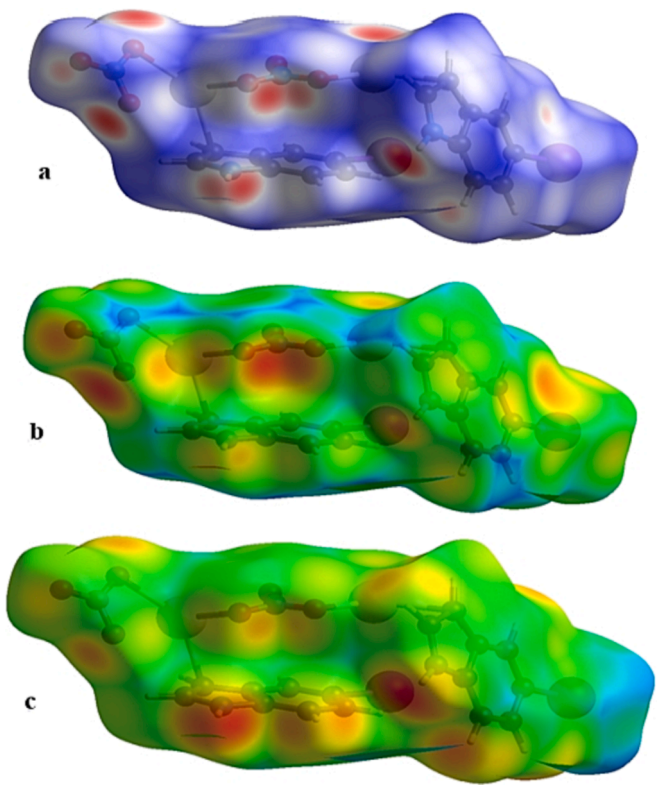

Fig. 7. The Hirshfeld surfaces of the $Ag_2(NO_3)_2(C_8H_6IN)_2$ mapped over d_{norm}, d_i and d_e.

atoms had less negative values. It was reported that the iodine atom of 5-iodoindole has a negative charge in the APT and Hirsfeld charge analysis. The same results were also found for the title complex in this study. When the complex is examined, it is seen that Ag metals also bond with the negative C atoms in the pyrrole ring of 5-iodoindole [48]. Furthermore, in the charge analysis research of the synthesized [Ag(3-Py-CHO)$_2$(NO$_3$)] compound, it is found O atoms in the nitrate group have negative values in Mulliken and NBO charge analyses, whereas Ag metal is positive [20]. These results support our study.

3.9. Non-linear optical properties

Recently, it has became very important to investigate the nonlinear optical properties of crystal structures and organic molecules due to their potential applications in research areas such as electrooptical switches, frequency conversion, color display, and optical information processing [77]. The reaction of electrons in the structure as a result of exposure to an electric field can be explained as the optical property of a substance. DFT calculations have become an effective method to explain polarizabilities, hyperpolarizabilities, dipole moment, and electronic charge distribution [53]. Therefore, in this study, its non-optical properties will be explained only by the theoretical calculation method. The dipole moment of a structure exposed to an external electric field is reshaped and is given by the following equation:

$$\mu(t) = \mu_0 + \alpha\beta E^2 + \frac{1}{2}\beta E^2 + \frac{1}{6}\gamma E^3 + \ldots \quad (4)$$

In this equation, μ_0 is the permanent dipole moment of the molecule, α is the molecular polarity, β is the first-order hyperpolarizability, and γ is the second-order hyperpolarizability [78]. The permanent dipole moment (μ), the mean polarizability ($\bar{\alpha}$), the anisotropy of the polarizability ($\Delta\alpha$) and first-order hyperpolarizability (β_0) values are calculated as follows [79,80]:

$$\mu^2 = \mu_x^2 + \mu_y^2 + \mu_z^2 \quad (5)$$

$$\Delta\alpha = \frac{1}{\sqrt{2}}[(\alpha_{xx} - \alpha_{yy})^2 + (\alpha_{yy} - \alpha_{zz})^2 + (\alpha_{zz} - \alpha_{xx})^2 + 6(\alpha_{xy}^2 + \alpha_{yz}^2 + \alpha_{xz}^2)]^{1/2} \quad (6)$$

$$\beta_0 = [(\beta_{xxx} + \beta_{xyy} + \beta_{xzz})^2 + (\beta_{yyy} + \beta_{xxy} + \beta_{yzz})^2 + (\beta_{zzz} + \beta_{xxz} + \beta_{yyz})^2]^{1/2} \quad (7)$$

Hyperpolarizability is the amount that affects the nonlinear optical properties of the material. The nonlinear optical properties of $Ag_2(NO_3)_2(C_8H_6IN)_2$ are tabulated in Table 8.

The first hyperpolarizability value of $Ag_2(NO_3)_2(C_8H_6IN)_2$ is calculated at 9.10×10^{-30} esu. In the calculations made using the same basis set for the free 5-iodoindole molecule, this value was found to be 1.20×10^{-30} esu. The complex formation of the free ligand with silver nitrate increased the NLO optical properties [48]. Also, this value is approximately 24 times greater than that of urea (0.3728×10^{-30} esu) used as a brink value in NLO characteristic analysis. Therefore, the title molecule has important non-linear optical properties.

3.10. Thermodynamic properties

For the title complex structure, the heat capacity (Cp), entropy (S), enthalpy changes (ΔH), and Gibbs free energies, which play crucial roles in the material characterization and in understanding the reactivity and environmental influences on the molecules, were calculated at constant pressure in the gas phase. The values of these functions calculated in the temperature range of 100–1000 K are given in Table 9, and their changes depending on the temperature are presented in supplementary Fig. S4. The zero-point energy, which is characteristic property of molecules, remains constant at all temperatures and was found to be 707. 74

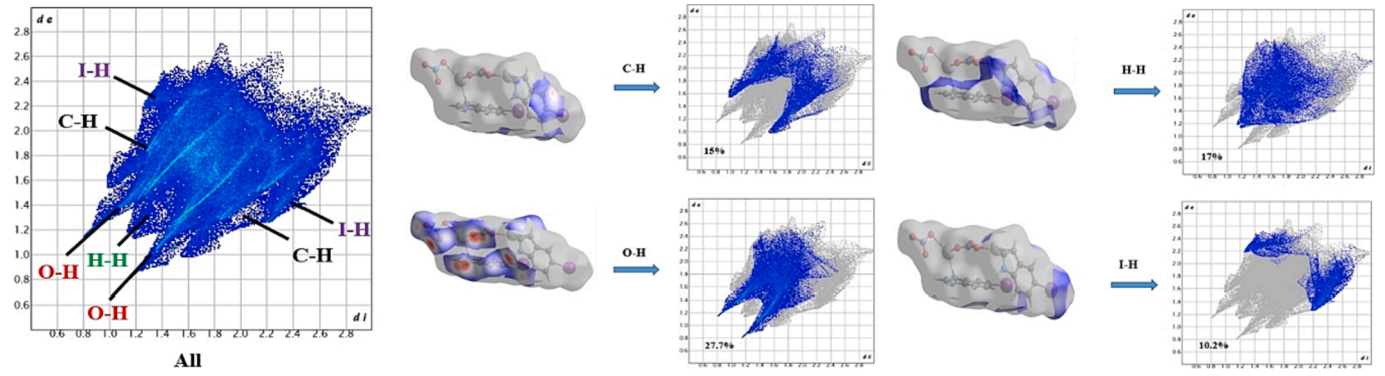

Fig. 8. Two-dimensional fingerprint plots order with a dnorm view of the O—H/H···O(27.7%), H···H (17%), C···H/H···C (15%) and I–H/H···I (10.2%) contacts in $Ag_2(NO_3)_2(C_8H_6IN)_2$.

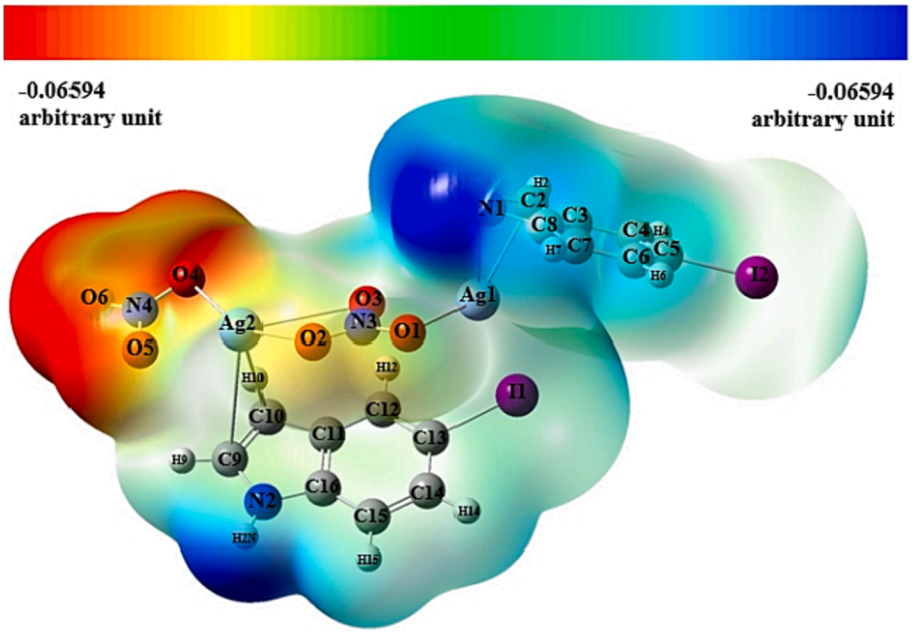

Fig. 9. Molecular electrostatic potential surface map of $Ag_2(NO_3)_2(C_8H_6IN)_2$ in the gas phase.

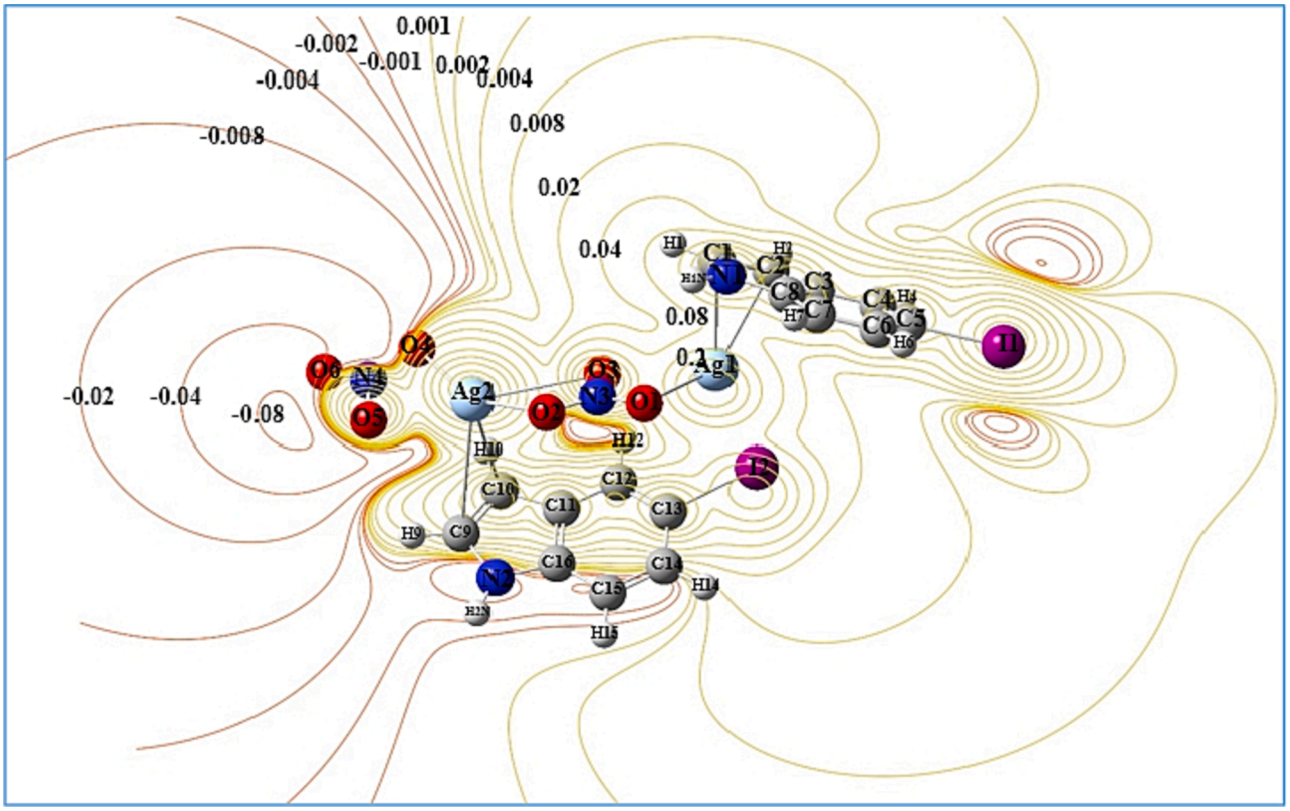

Fig. 10. Two dimensions contour map of molecular electrostatic potential surface values (all in arbitrary unit) of $Ag_2(NO_3)_2(C_8H_6IN)_2$.

kJmol^{-1}. For the synthesized complex structure, the lowest entropy, heat capacity and enthalpy change values were found to be 477. 50 Jmol^{-1}K^{-1}, 170.94 Jmol^{-1}K^{-1} and 2.57 kJmol^{-1} at 100 K, respectively, while the highest values were found as 1321 Jmol^{-1}K^{-1}, 590.76 Jmol^{-1}K^{-1} and 99.24 kJmol^{-1} at 1000 K. Entropy, heat capacity, and enthalpy change values showed an increase as the temperature rises. The increase in entropy and enthalpy due to the rise in temperature shows that the synthesized complex structure changes its thermodynamic system [48]. Also, Gibbs free energy value showed a decrease with increasing temperature.

3.11. Antimicrobial activity

The antibacterial activities of the title complex structure were tested

Table 7
Comparison of NBO, Hirshfeld and APT atomic charges for title compound.

Atoms	APT	Hirshfeld	NBO	Atoms	APT	Hirshfeld	NBO
Ag_1	0.752	0.212	0.623	C_8	0.175	0.047	0.152
Ag_2	0.848	0.216	0.756	C_9	0.115	0.024	0.032
I_1	−0.138	−0.101	0.178	C_{10}	−0.261	−0.069	−0.317
I_2	−0.170	−0.001	0.239	C_{11}	0.058	−0.013	−0.077
O_1	−0.748	−0.237	−0.476	C_{12}	−0.091	−0.037	−0.206
O_2	−0.740	−0.196	−0.483	C_{13}	0.268	0.028	−0.205
O_3	−0.708	−0.214	−0.524	C_{14}	−0.214	−0.051	−0.247
O_4	−0.799	−0.265	−0.565	C_{15}	0.042	−0.049	−0.205
O_5	−0.801	−0.266	−0.567	C_{16}	0.174	0.044	0.156
O_6	−0.785	−0.270	−0.415	H_1	0.107	0.079	0.233
N_1	−0.483	−0.069	−0.523	H_2	0.103	0.063	0.245
N_2	−0.455	−0.079	−0.536	H_3	0.259	0.164	0.418
N_3	1.317	0.277	0.706	H_4	0.067	0.056	0.223
N_4	1.468	0.259	0.691	H_5	0.069	0.056	0.223
C_1	0.078	0.034	0.001	H_6	0.042	0.059	0.220
C_2	−0.237	−0.061	−0.368	H_7	0.119	0.073	0.232
C_3	0.013	−0.016	−0.087	H_8	0.102	0.062	0.247
C_4	−0.093	−0.041	−0.214	H_9	0.076	0.061	0.226
C_5	0.287	0.034	−0.207	H_{10}	0.068	0.053	0.221
C_6	−0.189	−0.039	−0.221	H_{11}	0.032	0.055	0.216
C_7	0.029	−0.045	−0.204	H_{12}	0.240	0.157	0.408

Table 8
The electric dipole moment μ (Debye), average polarizability $\overline{\alpha}$, anisotropy of polarizability $\Delta\alpha$ ($10^{-24}esu$), and first hyperpolarizability β_0 ($10^{-30}esu$) of the title molecule.

Dipole moment		Polarizability		First Hyperpolarizability			
μ_x	4.39	α_{xx}	74.65	β_{xxx}	5.95	β_x	8.91
μ_y	1.22	α_{yx}	−6.58	β_{xxy}	−0.74	β_y	−0.14
μ_z	1.18	α_{yy}	42.38	β_{yxy}	1.73	β_z	−1.82
μ	4.71	α_{zx}	1.00	β_{yyy}	0.79	β_{tot}	9.10
		α_{zy}	−0.49	β_{xxz}	−0.46	$\overline{\beta}$	−1.09
		α_{zz}	42.50	β_{yxz}	−0.54		
		$\overline{\alpha}$	53.18	β_{yyz}	−0.66		
		$\Delta\alpha$	34.21	β_{zxz}	1.23		
				β_{zyz}	−0.19		
				β_{zzz}	−0.70		

Table 9
Thermodynamic properties at different temperatures of $Ag_2(NO_3)_2(C_8H_6IN)_2$.

T(K)	$C^0_{p,m}$(J/mol K^{-1})	S^0_m(J/mol K^{-1})	ΔH^0_m(kJ/mol)	ΔG_{corr}(kJ/mol)	ε_{ZPE}(kJ/mol)
100	170.94	477.50	2.57	671.62	707.74
200	251.88	627.11	8.03	616.03	707.74
300	328.56	747.30	15.18	547.21	707.74
400	396.19	853.76	24.05	467.12	707.74
500	451.36	950.18	34.40	376.91	707.74
600	494.43	1037.98	45.91	277.49	707.74
700	527.62	1118.08	58.34	169.70	707.74
800	553.43	1191.39	71.46	54.24	707.74
900	573.95	1258.79	85.13	−68.21	707.74
1000	590.76	1321.03	99.24	−197.16	707.74

$C^0_{p,m}$: Heat capacity, S^0_m: Entropy , ΔH^0_m: Entalphy changes, G_{corr}: Gibbs free energy, ε_{ZPE}: Zero point energy.

against bacteria, such as *E. coli* ATCC 25922, *K. pneumoniae* ATCC 13883, *S. dysenteriae* ATCC 11835, *P. aeruginosa* ATCC 27853, *S. typhimurium* ATCC 14028, *B. subtilis* ATCC 6633, *S. aureus* ATCC 25923, *E. faecalis* ATCC 29212, *L. monocytogenes* ATCC 7644, and *C. albicans* ATCC 10231 by using both agar well diffusion and microdilution methods. Antibacterial activity results of the title complex inhibition zone diameter (mm) and Minimal Inhibitory Concentration (MIC) are given in Table 10. $Ag_2(NO_3)_2(C_8H_6IN)_2$ complex structure was highly effective against gram-positive and gram-negative bacteria, with zones of inhibition (ZOI) ranging from 10 to 20 mm in diameter. The title compound highly inhibited S. aureus and P. aeruginosa (ZOI = 20 mm) (Table 10). All gram negative bacteria except *P. aeruginosa* ATCC ATCC 27853 were less sensitive to $Ag_2(NO_3)_2(C_8H_6IN)_2$ in the agar well diffusion study. The P. aeruginosa and S. aureus reference bacteria exhibited higher inhibition zones than the other reference bacteria. Gram-positive bacteria exhibited ZOI around 15–20 mm in diameter in agar well diffusion studies, while Gram-negative bacteria exhibited ZOI around 10 mm in diameter. The title complex shows strong antifungal activity on the reference strain of C. albicans in the agar well diffusion method with the highest inhibition sites in this study. $Ag_2(NO_3)_2(C_8H_6IN)_2$ only showed a good antimicrobial effect against *S. aureus* and *P. aeruginosa* (31.25 μg/ mL) in the MIC (1000 μg/m-1) evaluation. In antimicrobial susceptibility testing with the microdilution broth method, the gram-positive bacterium S. aureus and the gram-negative bacterium P. aeruginosa showed sensitivity to the diluted $Ag_2(NO_3)_2(C_8H_6IN)_2$ (100 μg/ml) in ethyl alcohol, and the minimal inhibitor concentration values were found to be 31.25. The synthesized complex structure with silver in this study can have promising applications in the biomedical, dentistry, and pharmaceutical fields. While 5-iodoindole showed no antimicrobial effect against E. coli, P. aeruginosa, and C. albicans [48], its silver nitrate complex showed strong antimicrobial activity against these bacterias. In other words, the binding of silver nitrate to the 5-iodiondole structure increased the antimicrobial effect.

4. Conclusion

In the present work, a new organic–inorganic hybrid compound, Ag2 (NO3)2(C8H6IN)2, has been synthesized at + 4°C by slow evaporation for 3 months. The molecular and structural properties of this new complex structure were determined by single-crystal X-ray diffraction techniques, Far-IR, FT-IR, FT-Ra, and ^{1}H NMR analayses. DFT calculations were carried out on an isolated molecule in the gas phase using B3LYP with the 6311++G (d, p) basis set for C, H, and N atoms and the DGDZVP basis set for Ag and I atoms. When the results are examined, it is found that there is a good correlation between the theoretical and experimental bond lengths, bond angles, and wavenumbers except for small differences. Also, the experimental and calculated ^{1}H NMR chemical shift values of the title structure are determined to be in good agreement with each other. Hirshfeld surface analysis and related two-dimensional fingerprint drawings have been performed to investigate the contributions of different intermolecular interactions in the crystal packing motif. The HOMO-LUMO energy gap value has been determined

Table 10
Results of antimicrobial activity of the $Ag_2(NO_3)_2(C_8H_6IN)_2$ the inhibition zone diameter (mm) and MIC values.

Microorganisms	Diameter of inhibition zone (mm)			MIC (1000 μg/m^{-1})
	$Ag_2(NO_3)_2(C_8H_6IN)_2$ (μg/mL)	AMP (10 μg)	Cycloheximide	$Ag_2(NO_3)_2(C_8H_6IN)_2$ (μg/mL)
E. coli ATCC 25922	10	–	–	125
K. pneumoniae ATCC 13883	10	18	–	250
S. dysenteriae ATCC 11835	10	24	–	125
P. aeruginosa ATCC 27853	20	18	–	31.25
S. typhimurium ATCC 14028	10	–	–	125
B. subtilis ATCC 6633	15	15	–	62.5
S. aureus ATCC 25923	20	20	–	31.25
E. feacalis ATCC 29212	15	15	–	62.5
L. monocytogenes ATCC 7644	15	–	–	62.5
C. albicans ATCC 10231	10	–	18	62.5

3.6 eV in the gas phase, and this energy value supports that this complex structure is a hard one. The molecular electrostatic potential (MEP), local reactivity descriptors, and charge analyses have been used to determine electrophilic and nucleophilic reaction regions. According to these analysis results, electrophilic regions are localized over the O atoms in the nitrate groups. NLO properties have been investigated and the first hyperpolarizability value has been obtained, 24 times greater than the urea used as a brink value. According to this result, the title molecule has the potential to be used as an NLO material. In antimicrobial activity studies, the complex structure has been highly effective against gram-positive and gram-negative bacterias. In particular, the title compound highly inhibits S. aureus and P. aeruginosa. Also, the title complex has been shown to exhibit strong antifungal activity on the reference strain of C. albicans in this study.

Declaration of Competing Interest

The authors declare that they have no known competing financial interests or personal relationships that could have appeared to influence the work reported in this paper.

Data availability

Data will be made available on request.

Acknowledgements

This study was supported by Ondokuz Mayıs University (Project No: PYO.FEN.1906.19.001).

Appendix A. Supplementary data

CCDC 2043732 contains the supplementary crystallographic data for the compound reported in this article. These data can be obtained free of charge on application to CCDC, 12 Union Road, Cambridge CB2 1EZ, UK [Fax: +44 1223 336 033, e-mail: deposit@ccdc.cam.ac.uk, https://www.ccdc.cam.ac.uk/structures/].

Supplementary data to this article can be found online at https://doi.org/10.1016/j.inoche.2023.110465.

References

[1] S. Tariq, A.R. Raza, M. Khalid, S.L. Rubab, U.K. Muhammad, A. Ali, M.N. Tahir, A. A.C. Braga, Synthesis and structural analysis of novel indole derivatives by XRD, spectroscopic and DFT studies, J. Mol. Struct. 1203 (2020), 127438.
[2] T.P. Pathak, K.M. Gligorich, B.E. Welm, M.S. Sigman, Synthesis and preliminary biological studies of 3-substituted indoles accessed by a palladium-catalyzed enantioselective alkene difunctionalization reaction, J. Am. Chem. Soc. 132 (23) (2010) 7870–7871.
[3] F. Bouchikhi, E. Rossignol, M. Sancelme, B. Aboab, F. Anizon, D. Fabbro, M. Prudhomme, P. Moreau, Synthesis and biological evaluation of diversely substituted indolin-2-ones, Eur. J. Med. Chem. 43 (11) (2008) 2316–2322.
[4] M. Giampieri, A. Balbi, M. Mazzei, P.L. Colla, C. Ibba, R. Loddo, Antiviral activity of indole derivatives, Antivir. Res. 83 (2) (2009) 179–185.
[5] M. Frederich, M. Tits, L. Angenot, Potential antimalarial activity of indole alkaloids, Trans. R. Soc. Trop. Med. Hyg. 102 (1) (2008) 11–19.
[6] M.A. Radwan, E.A. Ragab, N.M. Sabry, S.M. El-Shenawy, Synthesis and biological evaluation of new 3-substituted indole derivatives as potential anti-inflammatory and analgesic agents, Biorg. Med. Chem. 15 (11) (2007) 383.
[7] E. Abele, R. Abele, O. Dzenitis, E. Lukevics, Indole and Isatin Oximes: Synthesis, Reactions, and Biological Activity, Chem. Heterocycl. Compd. 39 (1) (2003) 3–35.
[8] T.V. Sravanthi, S.L. Manju, Indoles-A promising scaffold for drug development, Eur. J. Pharm. SCI. 91 (2016) 1–10.
[9] D. Lednicer, The organic chemistry of drug synthesis, John Wiley & Sons, 2007.
[10] O. Talaz, İ. Gülçin, S. Göksu, N. Saracoglu, Antioxidant activity of 5, 10-dihydroindeno [1, 2-b] indoles containing substituents on dihydroindeno part, Biorg. Med. Chem. 17 (18) (2009) 6583–6589.
[11] S. Lal, T.J. Snape, 2-arylindoles: a privileged molecular scaffold with potent, broadranging pharmacological activity, Curr. Med. Chem. 19 (28) (2012) 4828–4837.
[12] Z.A. Khan, S.A. Shahzad, A. Anjum, A.T. Bale, S.A.R. Naqvi, Syenthetic approaches toward the reserpine, Syent. Commun. 204 (2018) 1128–1147.
[13] R.E. Dolle, Comprehensive survey of combinatorial library synthesis, J. Comb. Chem. 3 (2001) 477–517.
[14] M.Z. Zhang, Q. Chen, G.F. Yang, A review on recent developments of indole-containing antiviral agents, Eur. J. Med. Chem. 89 (2015) 421–441.
[15] J. Blaising, S.J. Polayk, E.I. Pechuer, Arbidol as a broad-spectrum antiviral: an update, Antivir. Res. 107 (2014) 84–94.
[16] A. Kumari, R.K. Singh, Medicinal chemistry of indole derivatives: Current to future therapeutic prospectives, Bioorganic. Chem. 89 (2019), 103021.
[17] M. Negård, S. Uhlig, H. Kauserud, T. Andersen, K. Høiland, T. Vrålstad, Links between genetic groups, indole alkaloids and ecology within the grass-parasitic Claviceps purpurea species complex, Toxins (Basel) 7 (2015) 1431–1456.
[18] H.B. Liu, G. Lauro, R.D. O'Connor, K. Lohith, M. Kelly, P. Colin, G. Bifulco, C. A. Bewley, Tulongicin and antibacterial triindole alkaloid from a deep water topsentia sp. sponge, J. Nat. Prod. 80 (2017) 2556–2560.
[19] U.A. Khan, A. Badshah, M.N. Tahir, E. Khan, Gold(I), Silver(I) and Copper(I) Complexes of 2,4,6-trimethylphenyl-3-benzoylthiourea, Synthesis and biological applications, Polyhedron 181 (2020), 114485.
[20] S. Celik, S. Yurdakul, B. Erdem, Synthesis, spectroscopic characterization (FT-IR, PL), DFT calculations and antibacterial activity of silver(I) nitrate complex with nicotinaldehyde, Inorg. Chem. Commun. 131 (2021), 108760.
[21] H.H. Repich, S.I. Orysyk, V.V. Orysyk, Y.L. Zborovskii, V.I. Pekhnyo, M.V. Vovk, Synthesis, crystal structure and spectral characterization of the first Ag+ complex compounds involving O, N, O-coordinated N-acylhydrazones of salicylaldehyde, J. Mol. Struct. 1144 (2017) 225–236.
[22] C. O'Beirne, N.F. Alhamad, Q.M.H. Müller-Bunz, K. Kavanagh, G. Butler, X. Zhu, M. Tacke, Synthesis, structures and antimicrobial activity of novel NHC*- and Ph3P-Ag(I)-Benzoate derivatives, Inorg. Chim. Acta 486 (2019) 294–303.
[23] G. Achar, C.R. Shahini, S.A. Patil, J.G. Malecki, S. Pan, A. Lan, X. Chen, S. Budagumpi, Sterically modulated silver(I) complexes of coumarin substituted benzimidazol-2-ylidenes: Synthesis, crystal structures and evaluation of their antimicrobial and antilung cancer potentials, J. Inorg. Biochem. 183 (2018) 43–57.
[24] S.M. Soliman, S.E. Elsilk, Synthesis, X-ray structure, DFT and antimicrobial studies of Ag(I) complexes with nicotinic acid derivatives, J. Photoch. Photobio. B 187 (2018) 48–53.
[25] R.S. Joseyphus, M.S. Nair, Synthesis, characterization and biological studies of some Co(II), Ni(II) and Cu(II) complexes derived from indole-3-carboxaldehyde and glycylglycine as Schiff base ligand, Arab. J. Chem. 3 (2010) 195–204.
[26] O.Yamauchi, M. Takani, K. Toyoda, H. MasudaI, Indole Nitrogen-Palladium (11) Bonding. Chemical and Structural Characterization of Palladium (11) Complexes of Alkylindoles and Intermediacy of the 3H-Indole Ring, Inorg. Chem. 29 (1990) 1856-1860.
[27] M.J. Frisch, G. Trucks, H. Schlegel, G. Scuseria, M. Robb, J. Cheeseman, V. Barone, B. Mennucci, G. Petersson, et.al. Gaussian 09. Revision C.01; Gaussian, Inc.: Wallingford CT, 2009.
[28] R. Dennington, T. Keith, J. Millam, GaussView version 5, Semi-chem Inc., Shawnee Mission, KS, 2009.

[29] A.G. Yurieva, K.H. Poleshchuk, V.D. Filimonov, comparative analysis of a full-electron basis set and pseudopotential for the iodine atom in DFT quantum-chemical calculations of iodine-containing compounds, J. Struct. Chem. 49 (3) (2008) 548–552.

[30] M. Pousti, M. Abbaszadeh, M.S. Lashkenari, M.M. Ghorbani, A combined experimental and theoretical studies on molecular structure and vibrational spectra of polyaniline and polyaniline/silver nanocomposite, Synth. MetSynth. Met. 183 (2013) 63–68.

[31] J. Huang, G.G. Zhang, Y. Huang, D. Fang, D. Zhang, Density functional theory study on antiferromagnetic interactions in a silver (I) complex of nitronyl nitroxide, J. Magn. Magn. MaterJ. Magn. Magn. Mater. 299 (26) (2006) 480–486.

[32] L.E.H. Paul, I.C. Foehn, A. Schwarzer, E. Brendler, U. Böhme, Salicylaldehyde-(2-hydroxyethyl)imine – A flexible ligand for group 13 and 14 elementsSalicylaldehyde-(2-hydroxyethyl)imine – A flexible ligand for group 13 and 14 elements, Inorganica. Chim. Acta. 423 (A) (2014) 268–280.

[33] P.R. Spackman, M.J. Turner, J.J. McKinnon, S.K. Wolff, D.J. Grimwood, D. Jayatilaka, M.A. Spackman, CrystalExplorer: a program for Hirshfeld surface analysis, visualization and quantitative analysis of molecular crystalsCrystalExplorer: a program for Hirshfeld surface analysis, visualization and quantitative analysis of molecular crystals, J. Appl. Cryst. 54 (3) (2021) 1006–1011.

[34] NCCLS, Performance Standards for Antimicrobial Susceptibility Testing:13th Informational Supplement (Disk Diffusion Supplemental Tables). NCCLS document M100-S13 (M2), supplement to NCCLS document M2-A8 (disk diffusion), (2003).

[35] NCCLS, Performance Standards for Antimicrobial Susceptibility Testing: 10th Informational Supplement (Aerobic Dilution, MIC Testing Supplemental Tables. NCCLS document M100-S10(M7), supplement to NCCLS document M7-A5 (MIC testing), (2000).

[36] X-AREA (Version 1.18) and X-RED32 (Version 1.04) Stoe & Cie, Darmstadt, Germany, (2002).

[37] L. Palatinus, G. Chapuis, SUPERFLIP-A computer program for the solution of crystal structures by charge flipping in arbitrary dimensions, J. Appl. Crystallogr. 40 (2007) 786–790.

[38] G.M. Sheldrick, Crystal structure refinement with SHELXL, Acta. Crystallogr. C. 71 (2015) 3–8.

[39] O.V. Dolomanov, L.J. Bourhis, R.J. Gildea, J.A.K. Howard, H. Puschmann, A complete structure solution, refinement and analysis program, J. Appl. Crystallogr. 42 (2009) 339–341.

[40] L. Yang, D.R. Powell, R.P. Houser, Structural variation in copper(ı) complexes with pyridylmethylamide ligands: structural analysis with a new four-coordinate geometry index, τ_4, Dalton. Trans. 9 (2007) 955–964.

[41] A. Okuniewski, D. Rosiak, J. Chojnacki, B. Becker, Coordination polymers and molecular structures among complexes of mercury(II) halides with selected 1-benzoylthioureas, Polyhedron 90 (2015) 47–57.

[42] A.W. Addison, T.N. Rao, J. Reedijk, J.V. Rijn, G.C. Verschoor, Synthesis, structure, and spectroscopic properties of copper(II) compounds containing nitrogen–sulphur donor ligands; the crystal and molecular structure of aqua[1,7-bis(*N*-methylbenzimidazol-2′-yl)-2,6-dithiaheptane]copper(II) perchlorate, J. Chem. Soc. Dalton. Trans. 7 (1984) 1349–1356.

[43] J. Bernstein, R.E. Davis, L. Shimoni, N.L. Chang, patterns in hydrogen bonding: functionality and graph set analysis in crystals, Angew. Chem. Int. Ed. 34 (15) (1995) 1555–1573.

[44] M. Govindarajan, K. Ganasan, S. Periandy, M. Karabacak, S. Mohan, Vibrational spectroscopic analysis of 2-chlorotoluene and 2-bromotoluene: A combined experimental and theoretical study, Spectrochim. Acta. A. Mol. Biomol. Spect. (2015) 1005–1013.

[45] S. Celik, M. Alp, S. Yurdakul, A combined experimental and theoretical study on vibrational spectra of 3-pyridyl methyl ketone, Spectrosc. Lett. 53 (4) (2020) 234–248.

[46] R. Premkuma, R.M. Asath, T. Mathavan, A.M.F. Benial, Structural, vibrational spectroscopic and quantum chemical studies on indole-3-carboxaldehyde, AIP. Publ. 140041 (2017) 1–3.

[47] K.T. Mahendra, M.T. Rama, B. Alice, T. Dahryn, N. Gopal, M. Rakesh, bio-field treatment: a potential strategy for modification of physical and thermal properties of gluten hydrolysate and ıpomoea macroelementsbio-field treatment: a potential strategy for modification of physical and thermal properties of gluten hydrolysate and ıpomoea macroelements, J. Snehasis. (2015) J Environ Anal Chem 2(4): 1-8.

[48] C. Kucuk, S. Yurdakul, B. Erdem, Spectroscopic characterization, DFT calculations, and microbiological activity of 5-iodoindole, J. Mol. Struct. 1252 (2022), 132125.

[49] Y. Erdoğdu, O. Unsalan, D. Sajan, M.T. Gulluoglu, Structural conformations and vibrational spectral study of chloroflavone with density functional theoretical simulations, Spectrochim. Acta. A. 76 (2010) 130–136.

[50] Y. Erdogdu, D. Manimaran, M.T. Güllüoglu, M. Amalanathan, I.H. Joeb, S. Yurdakul, FT-IR, FT-Raman, NMR Spectra and DFT Simulations of 4-(4-Fluoro-phenyl)-1H-imidazole, Opt. Spect. 114 (4) (2013) 525–536.

[51] S. Srivastava, P. Gupta, A. Sethi, S.R. Pratap, One pot synthesis of Curcumin-NSAIDs prodrug, spectroscopic characterization, conformational analysis, chemical reactivity, intramolecular interactions and first order hyperpolarizability by DFT method, J. Mol. Struct. 1117 (2016) 173–180.

[52] S. Mohan, N. Sundaraganesan, FTIR and Raman studies on benzimidazole, Spectrochim. Acta. A. Mol. Biomol, Spectrosc. 47 (8) (1991) 1111–1115.

[53] S. Yurdakul, E. Temel, O. Buyukgungor, Crystal structure, spectroscopic characterization, thermal properties and theoretical investigations on [Ag(methyl 4-pyridylketone)2NO3], J. Mol. Struct. 1191 (2019) 301–313.

[54] M.T. Bilkan, S. Yurdakul, Experimental and Theoretical Studies on Molecular Structures and Vibrational Modes of Novel Compounds Containing Silver[1], Russ. J. Inorg. Chem. 62(7) 910-924.

[55] S. Ahmad, I. Georgieva, M. Hanif, M. Monim-ul-Mehboob, S. Munir, A. Sohail, A. A. Isab, Periodic DFT modeling and vibrational analysis of silver(I) cyanide complexes of thioureas, J. Mol. Model. 25 (2019) 90.

[56] V.I. Avdevv, G.M. Zhidomirov, Ethylene oxygen species adsorbed on a defect oxidized surface Ag(1 1 1) Theoretical analysis by DFT metod, Surf. Sci. 492 (2001) 137–151.

[57] H. Abe, K. Manzel, W. Schulze, Surface-enhanced Raman spectroscopy of CO adsorbed on colloidal silver particles, J. Chern. Phys. 74 (2) (1981) 791–798.

[58] O.H. Ellestad, P. Klaboe, E.E. Tucker, J. Songstad, The Vibrational Spectra and Molecular Structure of Some silver Pseudohalide Complex Anions, Acta Chem. Scand. 26 (1972) 3579–3592.

[59] S. Uzun, Z. Esen, E. Koç, N.C. Usta, M. Ceylan, Experimental and density functional theory (MEP, FMO, NLO, Fukui functions) and antibacterial activity studies on 2-amino-4- (4-nitrophenyl) -5,6-dihydrobenzo [h] quinoline-3-carbonitrile, J. Mol. Struct 1178 (2019) 450–457.

[60] H.E. Gottlieb, V. Kotlyar, A. Nudelman, NMR chemical shifts of common laboratory solvents as trace İmpurities, J. Org. Chem. 62 (1997) 7512–7515.

[61] E.R. Rangel, C. Torres, L. Rincón, S.K. Khatib, F.L. Carrasquero, copolymerizations of long side chain di n-alkyl itaconates and methyl n-alkyl itaconates with styrene: determination of monomers reactivity ratios by NMR, Rev. LatinAm. Metal. Mat. 32 (1) (2012) 79–88.

[62] M. Faizan, V.H.N. Rodrigues., S. Ahmad, Cocrystallization of 2,3-dimethylquinoxaline with 3,5-dinitrobenzoic acid: Crystal structure, Hirshfeld surface, spectroscopic features and DFT studies, J. Mol. Struct. 1198: 126.

[63] A. Hussain, M.U. Khan, M. Ibrahim, M. Khalid, A. Ali, S. Hussain, M. Saleem, N. Ahmad, S. Muhammad, A.G. Al-Sehemi, A. Sultan, Structural parameters, electronic, linear and nonlinear optical exploration of thiopyrimidine derivatives: A comparison between DFT/TDDFT and experimental study, J. Mol. Struct. 1201 (2020), 127183.

[64] S. Kumar, A. Radha, M. Kour, R. Kumar, A. Chouaih, S.K. Pandey DFT studies of disubstituted diphenyldithiophosphates of nickel(II): Structural and some spectral parameters, J. Mol. Struct. 1185 (2019) 212-218.

[65] S. Gece, Bilgiç, Molecular-level understanding of the inhibition efficiency of some inhibitors of zinc corrosion by quantum chemical approach, Ind. Eng. Chem. Res. 51 (2012) 14115–14120.

[66] H. Vural, M. Orbay, Synthesis, crystal structure, spectroscopic investigations and DFT calculations of the copper(II) complex of 4-(Trifluoromethyl)pyridine-2-carboxylic acid, J. Mol. Struct. 1146 (2017) 669–676.

[67] K. Balasubramani, G. Premkumar, P. Sivajeyanthi, M. Jeevaraj, B. Edisona, T. Swub, Crystal structure, Hirshfeld surface analysis and HOMO–LUMO analysis of (E)-4-bromo-N00-(4- methoxybenzylidene)benzohydrazide, Acta. Cryst. E. 74 (2018) 1500–1503.

[68] T.A. Shah, U. Alam, M.U. Alam, S. Park, M. Muneer, Single Crystal X-Ray Structure, Spectroscopic and DFT Studies of Imidazo [2,1- b]thiazole: 2-(3-Hydroxy-phenylimidazo[2,1-b]thiazol2(3H)-ylidene)-1-phenylethanone, J. Mol. Struct. 1157 (2018) 638–653.

[69] S.K. Seth, Structural elucidation and contribution of intermolecular interactions in *O*-hydroxy acyl aromatics: Insights from X-ray and Hirshfeld surface analysis, J. Mol. Struct. 1064 (2014) 70–75.

[70] R. Arulraj, S. Sivakumar, K. Rajkumar, J.P. Jasinski, M. Kaur, A. Thiruvalluvar, Synthesis, Crystal Structure, DFT Calculations and Hirshfeld Surface Analysis of 3-Chloro-3-methyl-r(2), c(6)-bis(p-methoxyphenyl) piperidin-4-one, J. Chem. Crystallogr. 50 (2020) 41–51.

[71] E.P. Cuadradoa, K. Ferrer, E. Osorioc, I. Brito, J. Cisterna, M. Gutiérrez, Crystal structure, Hirshfeld surface analysis and DFT studies of N-(4-acetylphenyl) quinoline-3-carboxamide, J. Mol. Struct. 1246 (2021), 131162.

[72] S. Xavier, S. Periandy, K. Carthigayan, S. Sebastian, Molecular Docking, TG/DTA, Molecular Structure, Harmonic Vibrational Frequencies, Natural Bond Orbital and TD-DFT Analysis of Diphenyl Carbonate by DFT Approach, J. Mol. Struct. 1125 (2016) 204–216.

[73] R.R. Saravanan, S. Seshadri, S. Gunasekaran, R.M. Mendoza, S.G. Granda, Conformational analysis, X-ray crystallographic, FT-IR, FT-Raman, DFT, MEP and molecular docking studies on 1-(1-(3-methoxyphenyl) ethylidene) thiosemicarbazide, Spectrochim. Acta. A. Mol. Biomol. Spect. 139 (2015) 321–328.

[74] M.A. Mumit, T.K. Pal, A. Alam, A.A.A.M. Islama, S. Paulb, M.C. Sheikh, DFT studies on vibrational and electronic spectra, HOMO–LUMO, MEP, HOMA, NBO and molecular docking analysis of benzyl-3N-(2,4,5-trimethoxyphenylmethylene) hydrazinecarbodithioate, J. Mol. Struct. 1220 (2020), 128715.

[75] A. Atilgan, S. Yurdakul, Y. Erdogdu, M.T. Güllüoğlu, DFT simulation, quantum chemical electronic structure, spectroscopic and structure-activity investigations of 4-acetylpyridine, J. Mol. Struct. 1161 (2018) 55–65.

[76] C. BardakC. Bardak, A. AtacA. Atac, F. Bardak F. Bardak Effect of the external electric field on the electronic structure, spectroscopic features, NLO properties, and interionic interactions in ionic liquids: A DFT approach, J. Mol. Struct. 2019, 273:314-325.

[77] S. Eryılmaz, N. Akdemir, E. İnkaya The examination of molecular structure properties of 4,4′-oxydiphthalonitrile compound: combined spectral and computational analysis approaches, Spectrosc. Lett. 52 (2016) 28-42.

[78] J. Leszczynski, M.G. Papadopoulos, A.J. Sadlej Non-Linear Optical Properties of Matter. Springer, Dordrecht, The Netherlands (2006).
[79] S.S.R.K.C. Yamijala, M. Mukhopadhyay, S.K. Pati Linear and Nonlinear Optical Properties of Graphene Quantum Dots: A Computational Study, J. Phys. Chem. C. 119 (2015) 12079-12087.
[80] S.K. Gunduz, B. Bicak, S. Celik, S. Akyuz, A.E. Ozel, Structural and spectroscopic investigation on antioxidant dipeptide, L-Methionyl-L-Serine: A combined experimental and DFT study, J. Mol. Struct. 1137 (2017) 756–770.